Future changes in extreme events in Mozambique as simulated using the PRECIS regional climate modeling system

Izidine S. de Sousa Pinto

Dissertation presented in partial

fulfilment of the requirements for the degree of

MASTER OF SCIENCE

in the Department of Environmental & Geographical Science

Supervisors: **Dr. Mark Tadross** and **Prof. Bruce Hewitson**

June 2011

Well it is going to fight with determination, embrace life and live with passion, lose with class and win with boldness, because the world belongs to those who dare, and life is much to be insignificant. I do and abuse of happiness and not give up my dreams. The world is in the hands of those who have the courage to dream and run the risk of living your dreams.

Charles Chaplin

Declaration

I know the meaning of plagiarism and declare that all of the work in the dissertation, save for that which is properly acknowledged, is my own.

. . . . . .

(**Izidine S. de Sousa Pinto**)

Abstract

Future climate change is generally believed to lead to an increase in climate variability and in the frequency and intensity of extreme events. Mozambique is well known for its occurrence of severe weather and extreme climate events such as floods, tropical cyclones and droughts. Such events have serious impacts on the livelihoods of most people who often rely on subsistence agriculture.

This dissertation explores possible changes in extremes in temperature and precipitation over Mozambique, based on high-resolution (25 km) simulations of the regional climate model system PRECIS (HadRM3P), forced by the ECHAM4 global model. Changes in extremes are discussed for the future 19-year period of 2031-2049 with respect to the present day period of 1981-1999 under an assumed A2 IPCC emission scenario. This study uses indices based on percentile thresholds and durations to describe extreme events of maximum and minimum temperature and precipitation on a season by season basis. Two different analyses of changes in each index are conducted. One examines spatial changes in grid point data, and the other compares empirical probability distribution functions (PDF) for three different periods (1981-1999, 2011-2029 and 2031-2049). A Self Organizing Maps (SOM) algorithm is used to classify the circulation patterns using 850 hPa geopontetial heights and relate changes in these circulation patterns to changes in extreme events in the future. The HadRM3P model is generally able to simulate the observed spatial patterns of temperature and precipitation. However there are some regions where the model underestimates/overestimates temperature and precipitation with respect the observations. A change in the intensity and distribution of daily temperature and precipitation towards more extreme events in particular regions is shown to likely occur under this scenario of increased greenhouse gas emissions and model configurations. In particular, the shift of the distribution of daily precipitation could have significant consequences resulting in increased incidences of floods in some regions.

Aknowledgements

Foremost I would like to sincerely thank both of my supervisors, Mark Tadross and Bruce Hewitson for their instruction, guidance, and generous assistance. From them I have learned a great deal, and without their ideas, comments, expertise, this dissertation would not have been possible. I wish to thank the Climate System Analysis Group (CSAG) and National Research Found (NRF) of the Republic of South Africa for providing financial support. I wish to acknowledge the British Met Office (Hadley Centre for Climate Prediction and Research, UK) for supplying the PRECIS modelling system. I am grateful to Dr. Pippin Anderson for support during the proposal development phase of this dissertation. I want to extend my gratitude to Dr. Ruth Cezero for invaluables comments and suggestions. I am indebted to the *CSAGers* for providing a conducive and interactive research environment and for their help to complete this dissertation. Thank you to Genito Maure who was always available to encourage and give general advice. Special thanks go to my mother for unconditional support in everything I do, my family members, my friends and almighty God for giving me the strength to challenge this complicated and unexpected but interesting profession.

List of Acronyms

CRU Climate Research Unit

DTR diurnal temperature range

ECMWF European Centre for Medium-Range Weather Forecast

ENSO El Niño-Southern Oscillation

GCM General Circulation Model

HadCM3 Hadley Centre Coupled Model version 3

HadRM3P Hadley Centre Regional Model version 3 and PRECIS Physics

INAM Instituto Nacional de Meteorologia

IPCC Intergovernmental Panel on Climate Change

ITCZ Inter Tropical Convergence Zone

LBC lateral boundary condition

MC Mozambique Channel

PDF Probability density functions

PRECIS **P**roviding **Re**gional **C**limates for **I**mpact **S**tudies

RCM Regional Climate Model

SD Statistical Downscaling

SOM Self-organising maps

SRES Special Report on Emissions Scenario

Contents

List of Tables

List of Figures

CHAPTER 1

Introduction

Increases in atmospheric greenhouse gases concentrations will result not only in changes in climate in the sense of average weather conditions, but also in changes in climate variability and extremes of weather conditions (IPCC, 2001). While changes in average conditions can have serious consequences by themselves, the main impacts of global climate change will be felt due to changes in climate variability and weather extremes. Changes in extremes events such as heat waves, heavy rain and droughts are responsible for a disproportionately large part of climate-related damages (Easterling et al., 2000; Meehl et al., 2000) and hence are of great concern to the community and stakeholders (Katz et al., 2005). There have been observed trends towards higher rainfall events (Fauchereau et al., 2003; New et al., 2006) and droughts that have persisted longer over southern African in recent years (Nicholson, 1985; Fauchereau et al., 2003). Such events have major impact on both human and natural systems, causing catastrophic losses of property and human life, regulating the spread of invasive species and exotic diseases, and acting as a direct agent of species extinction (Diffenbaugh et al., 2005). A possible increase in frequency of such events under climate change may exacerbate these impacts. Following this perspective, the analysis of extreme events in the present and future climate is of great importance.

Reliable projections of extreme events in a changing future climate are of vital interest to planners and policymakers due to the impacts that extreme events can have on human activities, agriculture and the economy. Modeling advances now provide the opportunity of utilizing General Circulation Models (GCMs) projections of extreme temperature and precipitation indicators (Tebaldi et al., 2006). However, the short term scale of extreme indicators cannot be adequately represented at the coarse spatial resolution of the GCMs (McGregor, 1997; Wilby and Wigley, 1997; Hudson and Jones, 2002). Dynamical downscaling from the GCM coarse resolution to a finer resolution is thus necessary to better resolve small-scale

weather events. Regional Climate Models (RCMs) are tools to add small-scale detailed information of future climate change to the large-scale projections of a GCM (Jones et al., 2004). These high-resolution dynamical RCMs nested in a GCM are becoming an increasingly important tool in climate research (IPCC, 2001). This study is focused on the application of a RCM, the main dynamical downscaling technique in exploring future extreme events over Mozambique.

1.1 The need for research over Mozambique

Mozambique is vulnerable to the effects of weather extremes (tropical cyclones, floods, droughts) in different ways. This is in part because it is a developing country with scarce financial and technical resources to face these climate events and their consequences (Ministério para a Coordenação da Acção Ambiental- MICOA, 2007). Because of its geographical location where as a low-lying coastal area in the global belt of arid and semi-arid areas of the world, it is particularly vulnerable to the impact of the climate change on living organisms, natural resources, the environment and consequently the national economy can be very severe (MICOA, 2007). Droughts tend to have a larger incidence in the southern areas, floods are more frequent in the centre and south, mainly along the rivers basins, whereas tropical cyclones strike the coastal zone (Instituto Nacional de Gestão de Calamidades - INGC, 2009). Regarding the duration of events, drought can prevail for long periods of time, up to three to four years; the effects of floods can last for some months, while cyclones last just few days. The floods are linked not only to local intense precipitation, but also to heavy water drainage from rivers in upstream neighbouring countries. Tropical storms and cyclones generally occur in summer and they can be particularly devastating bringing strong winds and torrential rain which cause floods, landslides, and coastal and inland erosion (MICOA, 2007). According to MICOA (2007), Mozambique is experiencing increases in the frequency and severity of droughts in the interior and floods in coastal regions. In 2000, Mozambique experienced the worst flooding events in many decades which left over 700 people dead and half a million homeless, destroyed infrastructures and millions of US Dollars in damage (Dyson and van Heerden, 2001).

The impacts of floods and droughts are diverse, for instance during droughts the vegetation dies and the land cover is reduced thus making the land more susceptible to erosion; during

the floods, the topsoil is washed away making it less fertile hence vegetation growth is reduced. The net result is the degradation of the environment leading to the reduction in natural resources, thus causing more suffering to Mozambique, especially to the poor who depend on natural resources to meet their needs. In this context, there is an obvious need to improve current knowledge of the extreme events of Mozambique. Together with this is a need to predict project changes in extreme events in the future, and the probable consequences on a regional and national scale. This demonstrates the need for more detailed regional simulations in comparison to the coarse resolution of GCM simulations. So far no regional scale climate change scenario simulations have been carried out over Mozambique, especially in relation to extremes events.

1.2 General Aspects of Mozambique

1.2.1 Geographical location and climate

Mozambique is situated on the Eastern coast of Southern Africa, between 10°27´S and 26°52´S latitudes and 30°12´E and 40°51´E longitudes. It borders the Republic of Tanzania to the north, Malawi, Zambia, Zimbabwe, South Africa and Swaziland to the west, and South Africa to the south. The east coast of Mozambique is on the Indian Ocean (Figure 1.1). The country spans an area of about 799,380 km^2, of which 98.4 ٪ is land and 1.6 ٪ is surface water. The largest area of the Mozambican territory is situated in the intertropical zone. As a result, the country is subject to four main factors of atmospheric circulation (Hurry and Heerden, 1982; Tyson and Preston-White, 2000; Tadross, 2009):

- the north-east airflow from the East African monsoon which crosses the equator and moves into eastern Africa, and south easterly trade winds off the Indian Ocean, the interface between these two air masses is regarded as being the Inter Tropical Convergence Zone (ITCZ);
- the semi-permanent South Indian Anticyclone and South Atlantic Anticyclone;
- thermal lows along the coast as result of the deepening of semi-permanent trough over Mozambique Channel during summer;
- and tropical storms and cyclones over the Mozambique Chanel.

Figure 1.1: Location and administrative division of Mozambique (source: DNA (1999))

According to Köppen´s classification of climate, four distinct tropical climates of humid tropical, dry tropical, semi-arid tropical and a modified climate due to elevation are found in Mozambique. The predominant climate is humid tropical, characterized by two seasons, a dry and relatively cold from April to October, and a hot and humid between November and March.

The rainfall has great spatial variability over the country. The coastal strip receives about 800 to 1000 mm of precipitation per year. South of Pemba gets less than 800 mm, and between Beira and Quelimane, precipitation is higher than 1200 mm. Because of the influence of the Northeast monsoon, which affects the north and centre of the country, and the influence of the high altitude, this area has mean annual rainfall of 1000 to 2000 mm, except the region between Tete and Chemba, where just 500 to 600 mm of rainfall occurs in average annually. The rainy season, which is hot and wet period, runs from November to March, and is followed by a dry and relatively cold season between April and October (Direcção

Nacional de Águas- DNA, 1999).

In the south of the country, the mean temperature varies between 23 °C in the coastal areas and 25 °C in the interior, where the climate is drier. In the north, temperature is general higher, with an annual mean of 25-26 °C in the lying coastal areas. In the higher areas, the temperature is lower: this is the case of the city of Lichinga in the northwest, located at 1200 meters above sea level, where the mean annual temperature is 18 °C. In the central region of the country, the mean annual temperature is 25 °C, but in upland areas it falls to 20 °C (DNA, 1999).

1.3 Aim and Objectives

The research in this dissertation seeks to understand potential changes in climate extremes over Mozambique by simulating present day as well as the future climate, using a high-resolution regional climate modeling system PRECIS for Mozambique. Specifically, the objectives of the study are to:

- estimate the model bias with respect to observational data;
- highlight periods and locations where extremes of temperature and precipitation may potentially increase;
- and link changes in the frequency and intensity of extreme events with changes in the driving atmospheric circulation.

1.4 Structure of the dissertation

After the introductory chapter, basic concept of extreme events and issues in modeling extreme events are summarized in chapter two. Chapter three outlines the methodology used in this research. The chapter attempts to offer a briefly model description, experimental design and the methods used to analyse the data. The results are presented and discussed in chapter four. In chapter five the concluding remarks are presented and future work are proposed.

CHAPTER 2

Background

2.1 Extreme Weather Events

Changes in climate variability and extremes of weather and climate events have received increased attention in the last few years (Folland et al., 2001). Understanding changes in climate variability and climate extremes is complex due to the interactions between the changes in the mean and variability (Meehl et al., 2000). Such interactions vary from variable to variable depending on their statistical distribution (Folland et al., 2001).

According to the Glossary of the Intergovernmental Panel on Climate Change (IPCC) Fourth Assessment Report (IPCC, 2007), an extreme weather event is defined as an event that is rare at a particular place and time of year. Definitions of rare varies, but an extreme event would normally be as rare as or rarer than the 10th or 90th percentile of the observed probability density function [1] of a given variable (e.g. temperature, precipitation, wind speed). By definition, the characteristics of what is called extreme weather may vary in space and time in an absolute sense. Single extreme events cannot be simply and directly attributed to anthropogenic climate change, as there is always a finite chance the event in question might have occurred naturally. When a pattern of extreme weather persists for some time, such as a season, it may be classed as an extreme climate event, especially if it yields an average or total that is itself extreme (e.g., drought or heavy rainfall over a season) (IPCC, 2007).

In order to gauge how changes in weather and climate extremes could influence society and ecosystems, it is useful to conceptually address how such extremes could change in a statistical sense. These statistical properties are captured by the probability distribution of a

[1] A probability density function is the distribution of the probabilities of all different possible weather or climate events

climate variable. For example, figure 2.1 presents a typical distribution of a climate variable that is normally distributed, such as temperature, and show how the tails of the distribution are anticipated to change in a warming world. Shaded areas indicate the extreme parts of

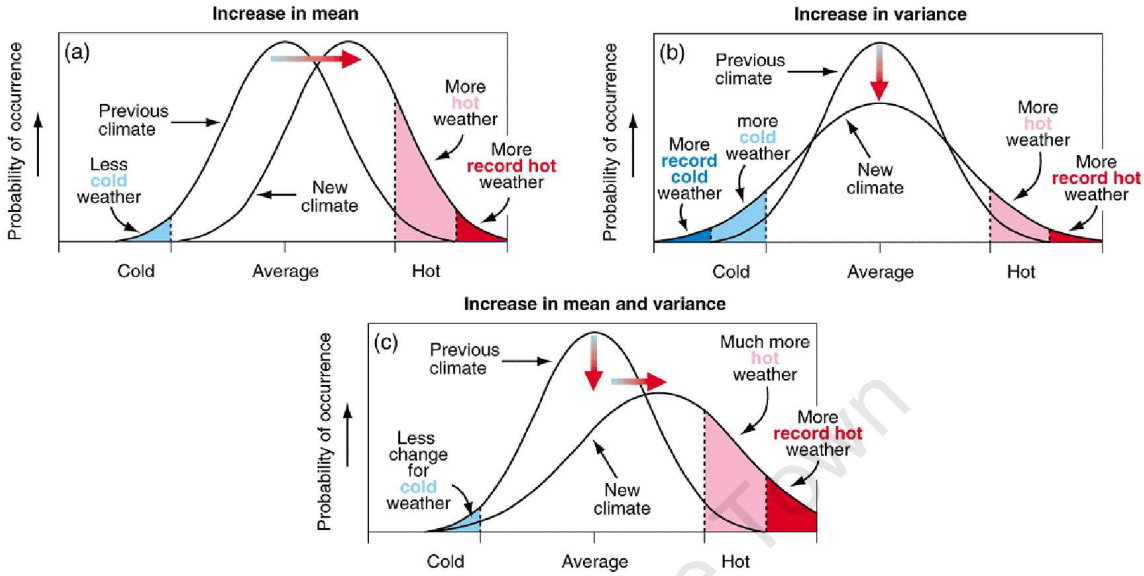

Figure 2.1: Theoretical changes in the normal distribution of climate variable (a) change in mean, (b) change in variance and (c) change in both mean and variance (source: IPCC, 2001).

the distribution, representing events in the tails of the distribution that are not frequent to occur. If there is a simple shift of the distribution in a future climate toward higher (warmer) values, there will be an increase in extremes events on one end and a decrease at the other (Figure 2.1a), such as an increase in mean will produce an increase in the number of extreme hot days and a decrease in the number of extreme cold days (Meehl et al., 2000). Consequently, there would be not only more hot weather but also more record hot and less cold weather. But a change in the mean does not imply any change in variability (IPCC, 2001). For example, in Figure 2.1a, the range between the hottest and coldest temperatures does not change. An increase in variability without a change in the mean implies an increase in the probability of both hot and cold extremes as well as the absolute value of the extremes (Figure 2.1b). According to Katz and Brown (1992), a change in the variance of a distribution will have a greater effect on the frequency of extremes events than a simple change in the mean. Increases in both the mean and the variability are also possible (Figure 2.1c), and affect the probability of hot and cold extremes, with more frequent hot events, more extreme high temperatures and fewer cold events (IPCC, 2001). According to the IPCC (2001) for variables that are not well approximated by normal distributions, like precipitation, the situ-

ation is even more complex, especially for dry climates. For example, changes in the mean total precipitation can be accompanied by other changes like the frequency of precipitation or the shape of the distribution including its variability. All these changes can affect the various aspects of precipitation extremes including the intensity of precipitation (amount per unit time).

Over many areas the frequency of heavy precipitation events has increased, consistent with warming, and widespread changes in extreme temperature observed over the last 50 years (IPCC, 2007). Several studies around the world have examined historical records for evidence of such trends. Klein Tank and Konnen (2003) investigated trends in temperature indices over Europe and found a symmetric warming of the cold and warm tails of the daily minimum and maximum temperature distributions during 1946 - 1999. Plummer et al. (1999) studied climate extremes in Australia and New Zealand during the 20th century and found increases in heavy rainfall, enhanced frequency of extreme warm days and nights, whilst extreme cool days and nights and drought events had decreased. Vincent et al. (2005) have found increasing trends in the percentage of warm nights and decreasing trends in the percentage of cold nights in South America during 1960-2000, and they attributed this mainly to more warm nights and fewer cold nights during the austral summer. New et al. (2006) analysed climatic extremes in southern and west Africa and reported that for Namibia, Botswana, Zambia and Mozambique extremely cold days and nights have decreased, and hot days and nights have increased, but maximum temperature is rising faster than minimum temperature extremes causing a increase in the diurnal temperature range (DTR). Additionally, they detected a decrease in total precipitation, accompanied by increased average rainfall intensity.

2.2 Climate modeling and extreme events

Understanding physical mechanisms of extremes involves processes governing the timing and location of extreme behaviour, such as El Niño-Southern Oscillation (ENSO) cycles, as well as the mechanisms of extremes themselves (e.g. processes producing heavy precipitation). This includes processes that create an environment conducive to extreme behavior, processes of the extreme behaviour itself, and the factors that govern the timing and location of extreme events.

As the resolution of climate models and the treatment of physical processes have improved, the simulation of extremes has also improved. Mainly because of increased data availability (e.g., daily data, various indices, etc.), modeling community has now examined the model simulations in greater detail and has presented a comprehensive description of extreme events in the coupled models used for climate change projections. State-of-the-art climate models are based on physical principles expressed as equations[2] solved by the model. Models solve these equations using one of two model formulations, grid point or spectral. However, each type formulates and solves the equations differently. The differences in the basic mathematical formulations lead to different methods for representing data. Grid point models represent data at discrete, fixed grid points, whereas spectral models use continuous wave functions. Global models are increasingly becoming grid point as computer resources increase [3]. There are also processes with scales too small to be resolved within the model grid. The model represents these processes through combinations of observations and physical theory usually called parameterizations. These parameterizations influence the climate model projections and are the source of a substantial fraction of the range associated with models projections of future climate.

2.2.1 General Circulation Models

General Circulation Models (GCMs) are tools used for studies of climate change and are able to appropriately reproduce the broad characteristics of current climate, including the general circulation patterns, temperature and synoptic scale precipitation (Daikaru, 2006) as well as large scale changes in the climate of the recent past; also they can represent large scale features such as ENSO and the Indian summer monsoon (Ashrit et al., 2001). However GCMs, present limitation when applied to extreme events studies. Some extreme events, by their very nature of being smaller in scale and shorter in duration cannot be adequately represented in a GCM grid box (Frei et al., 2006; Christensen et al., 2007a; Buonomo et al., 2007) due to the relatively coarse spatial resolution (which is usually about 300 x 300 km) of GCMs. Despite the concerns raised about their resolution, studies of climate extremes have been carried out using GCMs (e.g. Kiktev et al., 2003; Wehner, 2004; Kharin et al., 2005;

[2]Primitive equations: conservation of energy, conservation of momentum, conservation of mass and ideal gas law

[3]http://www.meted.ucar.edu/nwp/pcu1/ic2/frameset.htm?openTopic(1)

Emori et al., 2005). These GCMs studies of climate extremes are the starting point for most climate scenarios, however they lack the regional detail that impact studies generally need.

2.2.2 Downscaling

In view of need for regional projections, regionalization techniques have been developed to allow development of regional scale projections of change from the GCM output. There are two main approaches, statistical downscaling and dynamical downscaling.

Statistical Downscaling

Empirical or Statistical Downscaling (SD) is an alternative approach to obtaining regional-scale climate information (Hewitson and Crane, 1996; Wilby et al., 2004). Statistical Downscaling methods use cross-scale relationships that have been derived from observed data, and apply these to climate model data. Statistical Downscaling requires observational data at the desired scale for a long enough period to allow the method to be well trained and validated. Statistical Downscaling methods have the advantage of being computationally inexpensive, able to access finer scales than dynamical methods and applicable to parameters that cannot be directly obtained from the Regional Climate Model (RCM) outputs. The main drawbacks of SD methods are that they assume that the derived cross-scale relationships remain stable when the climate is perturbed, they cannot effectively accommodate regional feedbacks and, in some methods, can lack coherency among multiple climate variables (Christensen et al., 2007b).

Dynamical Downscaling

Dynamical downscaling uses Regional Climate Models (RCMs) to address the limitations of GCMs and statistical downscaling (Giorgi, 1990). RCMs are formulated using physical principles and they can realistically reproduce a broad range of climates around the world, which increases confidence in their ability to downscale probable future climates (Christensen et al., 2007b). The RCM is ``nested ´´within a GCM, this is done because RCMs cover only a portions of the planet, typically a continental domain or smaller, therefore they need to take information at their boundaries from GCMs or reanalyses data (e.g. NCEP, ERA40). Reanalyses are gridded data set representing the state of the Earth´s atmosphere, incorporating observations and numerical weather prediction (NWP) model output. Regional Climate

Model can represent the local land surface variable affecting regional climate as well as internal climate variations adding small-scale detailed information that impact studies generally need. Furthermore, they can represent extremes events better than GCMs on their grid-scale (Durman et al., 2001; Jones et al., 2004), for instance RCMs reproduce more precipitation extremes at scales not accessible to GCMs (e.g. Frei et al., 2003; Huntingford et al., 2003) as well as cyclones (Hudson and Jones, 2002).

The main advantages of these techniques are that they provide high resolution information on a large physically consistent set of climate variables and better representation of extreme events (Jones et al., 2004). The main drawbacks of dynamical models are their computational cost and that in future climates the parameterization schemes they use to represent sub-grid scale processes may be operating outside the range for which they were designed (Christensen et al., 2007b).

2.2.3 Emission scenarios

It is necessary to make assumptions on what the future will be like to better represent the climate system´s interactions. Several scenarios are derived from models projecting the future population, energy and the socio-economic interactions. The IPCC published a set of scenarios which are based on four different narrative storylines labeled A1, A2, B1 and B2. The A1 storyline is characterized by a future world of very rapid economic growth, a global population that peaks in mid-century and then gradually declines, and the rapid introduction of new and more efficient technologies. The A2 scenario describes a very heterogeneous world with a continuously increasing population and regionally oriented economic development that is more fragmented and slower than in other storylines. The B1 storylines is of a world more integrated, and more ecologically friendly characterized, with a convergent world with the same population as in the A1 storyline, but with rapid changes towards a service and information economy. The B2 storyline is of a world more divided in which the emphasis is on local solutions to economic, social and environmental sustainability, with continuously increasing global population, at a rate lower than A2, intermediate levels of economic development (Nakicenovic et al., 2000).

2.2.4 Uncertainties

There are several major uncertainties when dealing with climate projections, because a model can never fully describe the system that it attempts to simulate (Stainforth et al., 2007; Jones et al., 2004). The important sources of uncertainty that currently limit the detail of the regional projections are:

- Future emissions - projections of human behaviour and emissions of greenhouse gases are unpredictable;
- Uncertainty in the science - limited understanding and imperfect representation of key processes and feedbacks in climate models;
- Natural variability - any change, whether natural (e.g. solar activity, volcanic eruptions) or anthropogenic (e.g. land surface changes, greenhouse gases), in the components of the climate system and their interactions, or in the external forcing, may result in climate variations;
- Regionalisation technique (downscaling) - different approach of downscaling can give different local projections, even when based on the same GCM output.

CHAPTER 3

Model, Data and Methods

3.1 Model description

PRECIS (**P**roviding **Re**gional **C**limates for **I**mpact **S**tudies) is a regional climate modeling system developed by the Hadley Centre with Hadley Centre Regional Model version 3 and PRECIS Physics (HadRM3P) at the core. The PRECIS RCM system consists of a coupled atmospheric and land surface model describing processes related to dynamical flow, atmospheric sulfur cycle, clouds and precipitation, radiative processes, and the land surface and deep soil (Jones et al., 2004). The atmospheric component of HadRM3P model is based on the atmospheric component of the Hadley Centre´s state of the art coupled model HadCM3 (Gordon et al., 2000) with substantial modifications to the model physics. The land surface component employs the scheme MOSES (Met Office Surface Exchange Scheme, Cox et al. (1999)). The HadRM3P uses the grid scale dynamics and sub-grid physics similar to HadCM3 GCM. Owing to this the RCM provides high resolution simulations generally consistent with the large scale simulation of the parent GCM.

The atmospheric component of HadRM3P RCM is a hydrostatic version of the full primitive equations, i.e. vertical acceleration in the atmosphere is assumed to be small of hydrostatic equilibrium and hence vertical motions are diagnosed separately from the equations of state. It has a complete representation of the Coriolis force and employs a regular latitude-longitude grid in the horizontal and a hybrid vertical coordinate. The model has 19 atmospheric levels in the vertical (up to 30 km from surface) and four levels in the soil. The vertical coordinates are σ-p hybrid coordinate system with terrain following σ-coordinate (σ=pressure/surface pressure) at the lower four levels of the atmosphere transitioning to pressure coordinates at the top three levels of the atmosphere and a combination in between. The model equations

are solved in a spherical polar coordinates and the latitude-longitude grid is rotated so that the equator lies inside the region of interest in order to obtain quasi-uniform grid box area throughout the region (Jones et al., 2004).

HadRM3P can be run at two different horizontal resolutions, namely a 0.44°x 0.44° lat/lon and a 0.22°x 0.22° lat/lon (giving grid spaces of approximately 50km and 25km, respectively), requiring a timestep of 5 minutes for lower resolution and 2.5 minutes for a high resolution in order to maintain numerical stability (Jones et al., 2004). An Arakawa B grid (Arakawa and Lamb, 1977) is used for horizontal discretization to improve the accuracy of the split-explicit finite difference scheme. In this horizontal layout, the wind variables (zonal and meridional wind components) are offset by half a grid box in both directions from the thermodynamic variables (surface pressure, temperature and humidity) and aerosol variables.

HadRM3P requires prescribed surface and lateral boundary condition (LBC) at the edges of the regional domain to provide information about atmospheric dynamics for the RCM to run. Surface boundary conditions (time series of sea surface temperature and sea ice extents) are only required over water points. The main variables (prognostic variables) comprising the lateral boundary conditions for RCMs (including most Hadley Centre RCMs) are surface pressure, horizontal wind components, temperature and humidity through the depth of the atmosphere (Jones et al., 2004). Also, HadRM3P includes a representation of the sulphur cycle and so the relevant chemical species are also required as boundary conditions to simulate the spatial distribution of sulphate aerosols. The lateral boundary conditions are updated every six hours, while surface boundary conditions are updated once per model day. There is no prescribed constraint at the upper boundary of the RCM. The model uses a relaxation method (Davies and Turner, 1977) that is implemented across a four-point buffer zone at each vertical level. Values in the HadRM3P are relaxed towards the values interpolated in time from data saved every 6 hours from the GCM integration (Jones et al., 2004).

Regarding parameterizations, HadRM3P uses the prognostic variables to derive diagnostic variables. The latter consist of information on clouds, precipitation, atmospheric aerosols, boundary layer processes, land surface processes and gravity wave drag. Precipitation is modeled as large scale movement of air masses and as a result of convection. Cloud formation is calculated from simulated atmospheric profiles of temperature, pressure, humidity

and aerosol concentration. The conversion of cloud water to precipitation depends on the amount of cloud water present and precipitation falling into the grid box from above, causing a seeder-feeder enhancement Jones et al. (2004). A full description of the model and its parameterizations schemes are documented in Jones et al. (2004).

PRECIS has been used to develop regional climate change scenarios worldwide (e.g. Tadross et al., 2005; Rupa Kumar et al., 2006; Xu et al., 2006) including studying extremes (e.g. Zhang et al., 2006; Islam et al., 2009; Marengo et al., 2009).

3.1.1 Experimental Design

Two different simulations were performed to analyze present and future climate change in Mozambique. The first simulation was a 20-year (1 December 1979 to 31 December 1999) control run, which provides the baseline climate for model validation. In the first simulation HadRM3P was driven by ERA-40 (Uppala et al., 2005) reanalysis boundary data (hereafter referred to as Had/ERA). In the second simulation HadRM3P was run continuously for 71 years (from 1 December 1979 to 31 December 2050) with ECHAM4/OPYC3 (Roeckner et al., 1996; Oberhuber, 1993) as boundary condition using IPCC Special Report on Emissions Scenario (SRES) A2 scenario (Nakicenovic et al., 2000). HadRM3P driven by ECHAM4/OPYC3 under SRES A2 scenario (hereafter referred to as Had/ECHAM_A2) allow HadRM3P to be integrated continuously from the recent past to the middle of the 21st century, thus allowing periods such as the 2020s to be downscaled directly by the regional climate model, rather than relying on pattern scaling techniques (Wilson et al., 2008).

The domain chosen for the study roughly stretches over 29.9° S to 5.9° S and 27.5° E to 55.2° E and in total there are 110 grid points in latitude and 127 grid points in longitude covering Mozambique (Fig. 3.1) with spatial resolution of 0.22°x 0.22° where a more realistic topography is expected. Important to note that in the choice of an RCM domain, it is recommended to select a domain that is large enough so that the regional model can develop its own internal regional-scale circulations (Jones et al., 1995; Jones et al., 2004), but not too large that the climate of the RCM deviates significantly from the GCM in the centre of the domain (Leduc and Laprise, 2009). The model requires at least one year for a spin-up period to bring soil variables in the land surface model in equilibrium with the atmospheric forcing. As a result, data from the spin up period were not used in any analysis.

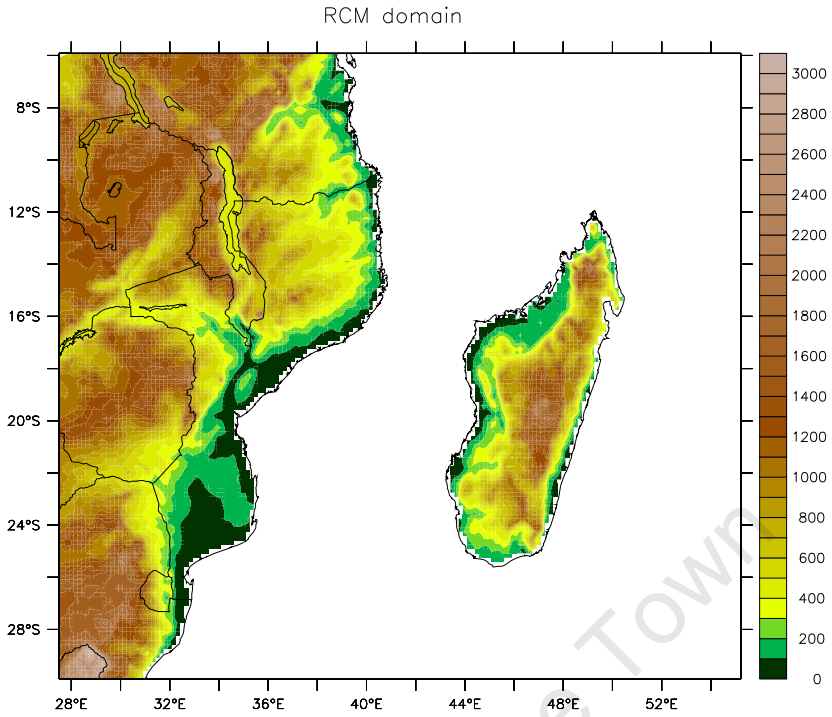

Figure 3.1: Regional model domain orography (m) on the regular latitude-longitude coordinate system.

3.2 Data

3.2.1 Lateral Boundary Conditions

Lateral boundary conditions (LBC) for HadRM3P are available from a range of model and observationally based sources and here LBC from the ECHAM4/OPYC3-coupled ocean-atmosphere GCM and ERA-40 reanalysis project were used.

The atmospheric general circulation model (ECHAM4) which provides the boundary fields for the HadRM3P simulations is the fourth version of the Hamburg climate model, which is based on the European Centre for Medium-Range Weather Forecast (ECMWF) weather forecast model. Prognostic variables are vorticity, divergence, surface pressure, temperature, water vapour and cloud water. ECHAM4 is a spectral model with a triangular truncation at wave number 42, which is equivalent to a horizontal resolution of about 2.8 degrees. Water vapour and cloud water are advected using a semi-Lagrangian scheme. A detailed description of the ECHAM4 model can be found in Roeckner et al. (1996). The ocean general circulation model OPYC3 is a version of the isopycnal model, the name is derived from

Ocean and isoPYCnal co-ordinates and use isopycnals as the vertical co-ordinate system. The model is described by Oberhuber (1993). When RCMs are forced with boundary conditions from GCMs, however, these boundary conditions often introduce systematic biases in the simulation of the present climate (Noguer et al., 1998). For this reason, the model is first tested using analyses of observations, i.e., so-called "perfect boundary conditions" (in this case ERA-40), although being a product of model simulations, the analyses of observations can still be affected by significant biases (Giorgi and Mearns, 1999). ERA-40 is a reanalysis of meteorological observations produced by the ECMWF. It covers the period from September 1957 to August 2002, has a horizontal resolution of 1.875 by 1.25 degrees (~187.5 by 125 Km) and is extensively described by Uppala et al. (2005).

3.2.2 Observational Data

For validation purpose the global surface climatology produced by the Climate Research Unit (hereafter CRU) of the University of East Anglia (New et al., 1999, 2000) and meteorological stations data supplied by the Instituto Nacional de Meteorologia (INAM) were used. The first includes monthly data of precipitation (ppt), minimum temperature (T_{min}) and maximum temperature (T_{max}) over land at a regular 0.5° resolution grid for the period 1901-2001, out of which data for 1981-1999 was extracted for comparison with the model simulation. CRU data suffers from errors in observed climatic averages for multi-decadal periods in the order of 0.5-1.3°C for temperature and 10-25% for precipitation. These errors are largest over regions characterized by scarce spatial coverage of stations (e.g. much of Africa) and high spatial variability (New et al., 1999, 2000). Nevertheless, this database has become a reference for validation of present climate modeling simulations (Hudson and Jones, 2002; Giorgi et al., 2004; Solman et al., 2008; Pesquero et al., 2009). The INAM stations consists of daily observed ppt, T_{min} and T_{max} for the period 1960-2006, from which the same period was extracted. Figure 3.2 shows the location of the 32 stations contained data for all, or a part of, this period.

3.3 Validation design

Four seasons were considered: austral summer (December, January and February - DJF), austral autumn (March, April and May - MAM), austral winter (June, July and August -

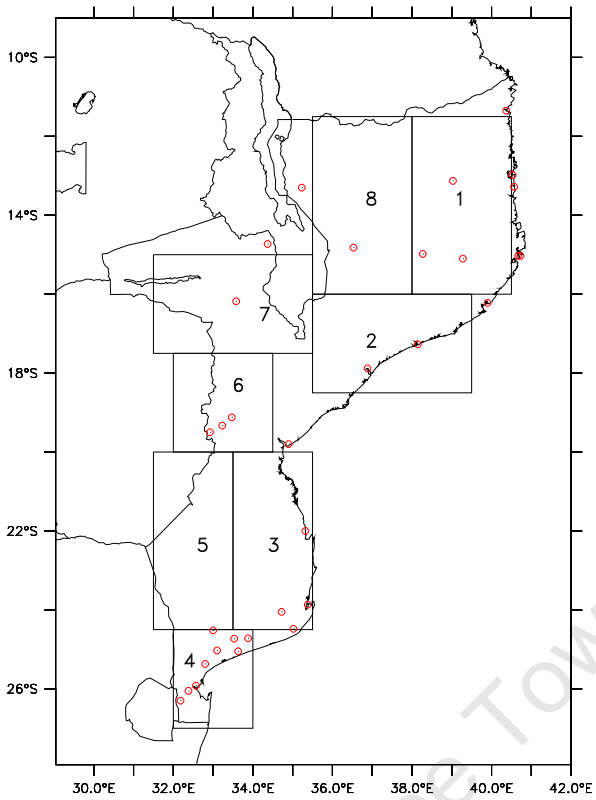

Figure 3.2: Locations of observed precipitation, minimum and maximum temperature stations (red circles) over Mozambique. The boxes indicate the sub-regions used for a more detailed analysis of the changes in PDF for temperature and precipitation.

JJA) and austral spring (September, October and November - SON). Several analysis were employed here for model validation. First a comparison of seasonal climatological means of CRU versus Had/ERA and Had/ECHAM_A2 was carried out. The CRU dataset is gridded which make it comparable to the model output allowing model validation. Validation of model output data with station data is not reliable as a consequence of limited spatial coverage of station network in Mozambique, i.e., approximately one station every 29000 km^2 (in South Africa this ratio is approximately one station every 1000 km^2 (Tadross, 2009)) as well as gaps appearing in station time-series data. On the other hand, station data by their nature as punctual measurements, are not directly comparable to the gridded model output such as HadRM3P. For this reason, station data was used to make qualitative comparisons of probability distribution function (PDF) of temperature and precipitation against model simulations over Mozambique. In comparisons of the PDFs all the 32 stations were included and the data did not undergone quality control, as Perkins et al. (2007) state that PDFs are less likely to be affected by observations errors compared to standard deviation or mean.

The model output (precipitation, maximum and minimum temperature) was linearly interpo-

lated to the CRU grid (0.5°) to make comparison possible, and all fields are shown over land only.

As a measure of the model systematic error the model bias was used (Equation 3.1), which is defined as the difference between all season average of Had/ERA in a 19-year period simulated and observed fields (from CRU dataset), i.e, Had/ERA minus CRU. In order to assess errors due to lateral boundary conditions the Echam bias was calculate (Equation 3.2), defined as the difference between the bias caused by Had/ECHAM_A2 and Had/ERA. The Echam bias represent the error introduced by the forcing ECHAM4/OPYC3 through the LBC.

$$HadRM3PBias = Had\_ERA - CRU \tag{3.1}$$

$$EchamBias = Had\_ECHAM\_A2 - Had\_ERA \tag{3.2}$$

where Had_ERA is the HadRM3P RCM driven by ERA-40 and Had_ECHAM_A2 is the HadRM3P RCM driven by the ECHAM4/OPYC3 GCM .

3.4 Future change of simulated extremes

The indices used in this study are suggested by the climate community coordinated by the joint WMO Commission for Climatology and the Expert Team on Climate Change Detection, Monitoring and Indices (ETCCDMI) of the Climate Variability and Predictability (CLIVAR) project (World Climate Research Programme), for temperature and precipitation extremes to gain insight to changes in extremes. From twenty-seven indices eight of them were used based on daily temperature values (minimum, maximum) and daily precipitation amount. The use of daily data is essential to describe timescales appropriate for variability description and societally sensitive extremes (Jones et al., 1999). The indices are calculated on the basis of percentile thresholds.

As a measure of intensity and frequency for extreme temperature conditions, the 90^{th} and 10^{th} percentile of maximum temperature and 90^{th} and 10^{th} percentile of minimum temperature of the daily data corresponding to the seasons of the 19-year modeled period (90×19=1710 data at each model point) have been computed. For events of extreme precipitation, the daily 95^{th} and 99^{th} precipitation percentile of wet-days was also considered. A threshold of 1.0 mm day^{-1} (e.g. New et al., 2006) is used to select wet days for the estimation of the 95^{th} and 99^{th} percentiles. The threshold of 1 mm was subjectively chosen to represent a measurable

quantity of rain. The extreme temperature indices used in the analysis are listed and defined in table 3.1. Of the four extreme precipitation three of them relate to “wetness”(R95p, R99p and CWD) while one of them relates to “dryness”(CDD). The CDD index is a measure of the length of the driest part of the multiannual season; this indicator may serve as a valuable drought indicator.

The indices were calculated for the present period 1981-1999 (CTL) and for the future period 2031-2049 (SCN), employing model data on a seasonal basis. Then, the differences between SCN and CTL were computed for all indices (SCN minus CTL). The advantage of percentiles is that they are comparable among the varying climates of the globe.
For a more detailed analysis of changes in the statistical distribution (PDFs) of daily mean maximum temperature, daily mean minimum temperature and daily mean precipitation the country were divided over several sub-regions defined in Figure 3.2. Here a new period was defined as 2011-2029 (MDL) to compare the changes throughout time.
The PDFs are obtained by simply computing the frequency of events across its range to produce a histogram. The results are then normalised to sum one, providing the estimated probabilities rather than the frequency distribution.
Comparing differences in pairs of probability distribution functions allows changes in all parts of the probability distribution to be investigated, including the extreme tails. This is motivated by the objective to explore possible future changes in the distributions of meteorological variables due to climate change.

The method chosen to determine changes in the atmospheric circulation and then link these to changes of extreme events was the artificial neural network system of self-organising maps (SOM), described in detail by Kohonen (2001). The SOM was used to determine the dominant synoptic types over Mozambique. The software used to create the SOM is SOM_PAK version 3.2 (Kohonen et al., 1996), available from http://www.cis.hut.fi/research/som-research. The SOM method was chosen because the types it produces represent the expected synoptic situations well and the data are evenly spread across the different types. Geopotential height is commonly used to characterize the circulation over southern Africa (e.g. Tyson and Preston-White, 2000). Each day can be matched to a particular synoptic type in the SOM. These features of the SOM allow analysis of the frequency of specific types of systems

Table 3.1: Climate extreme indices presented and discussed for Mozambique

	Index	Definition	Unit
Temperature indicators			
	Tx90p	90^{th} percentile of maximum temperatures	°C
	Tx10p	10^{th} percentile of maximum temperatures	°C
	Tn90p	90^{th} percentile of minimum temperatures	°C
	Tn10p	10^{th} percentile of minimum temperatures	°C
	Txf90	percent of time $T_{max}>90^{th}$ percentile of daily maximum temperature	% of time
	Txf10	percent of time $T_{max}<10^{th}$ percentile of daily maximum temperature	% of time
	Tnf90	percent of time $T_{min}>90^{th}$ percentile of daily minimum temperature	% of time
	Tnf10	percent of time $T_{min}<10^{th}$ percentile of daily minimum temperature	% of time
Precipitation indicators			
	R95p	95^{th} percentile of rainday amounts	mm/day
	R99p	99^{th} percentile of rainday amounts	mm/day
	CWD	Maximum number consecutive wet days (precipitation > 1 mm)	days
	CDD	Maximum number consecutive dry days (precipitation < 1 mm)	days

through time. A review of SOMs and the application to synoptic climatology is described in detail by Hewitson and Crane (2002). The size of the SOM array has a strong influence on the range of synoptic situations represented. The fewer the number of nodes in the SOM array the more general each pattern must be, while with a greater number of nodes a wider range of situations can be represented. A rectangular 7x5 array was chosen, following the work of Hewitson and Crane (2002), allowing 35 generalized synoptic states. Smaller or larger SOM arrays may be used, however, 35 states are considered adequate to capture all the expected synoptic types over Mozambique. Here, the SOM is trained on mean daily 850 hPa geopotential height fields of the Had/ERA for 1981-1999. Each day is therefore mapped to a particular SOM node and is associated with the same day of the Had/ECHAM_A2 for both control (CTL) and future (SCN) simulations. The procedure to train the SOM begins with a random initialization of the SOM array, followed by a two step training process with passes of 50000 iterations each. For the first training process the learning rate[1] was set to 0.05 and the initial radius of training area set to five which decreases linearly to one during training. On the contrary, the second training process the initial radius was set to three, with

[1]The measure of how much a node vector is adjusted to a data sample

a training rate of 0.025. The second training process develops the finer aspects of the SOM array.

CHAPTER 4

Results

4.1 Evaluation of model climatology

The climatological features of the present climate (1981-1999, CTL) in Mozambique derived from HadRM3P are discussed in this section. The objective is to provide an evaluation of the model performance in simulating the past climate. In the following analysis the model output (from Had/ECHAM_A2 and Had/ERA) is compared against observations (CRU) for each of the four austral seasons, summer (December-January, DJF), autumn (March-May, MAM), winter (June-August, JJA) and spring (September-November, SON). In the comparison of precipitation and surface temperature, the model output was interpolated to the CRU grid. The results are shown over land only since the CRU data is available over land.

Figures 4.1 and 4.2 show the maximum temperature (T_{max}) and minimum temperature (T_{min}) climatology comparisons of model output with observations. In all figures Had/ERA and Had/ECHAM_A2 capture the broad structure of the observed temperature fields and the locations of maximum and minimum for both T_{max} and T_{min}. In the north of the country is observed that both Had/ECHAM_A2 and Had/ERA overestimate Tmax during all seasons. In winter (JJA), the T_{max} and T_{min} is largely overestimated whereas during DJF they are largely underestimated by both simulations, indicating the bias resides within the HadRM3P model simulations. In some regions, Had/ECHAM_A2 and Had/ERA simulations closely agree with each other, however Had/ECHAM_A2 tends to exhibit the largest differences. In general, minimum temperatures are better represented than maximum temperatures, except during SON when Had/ECHAM_A2 simulates too high T_{min}.

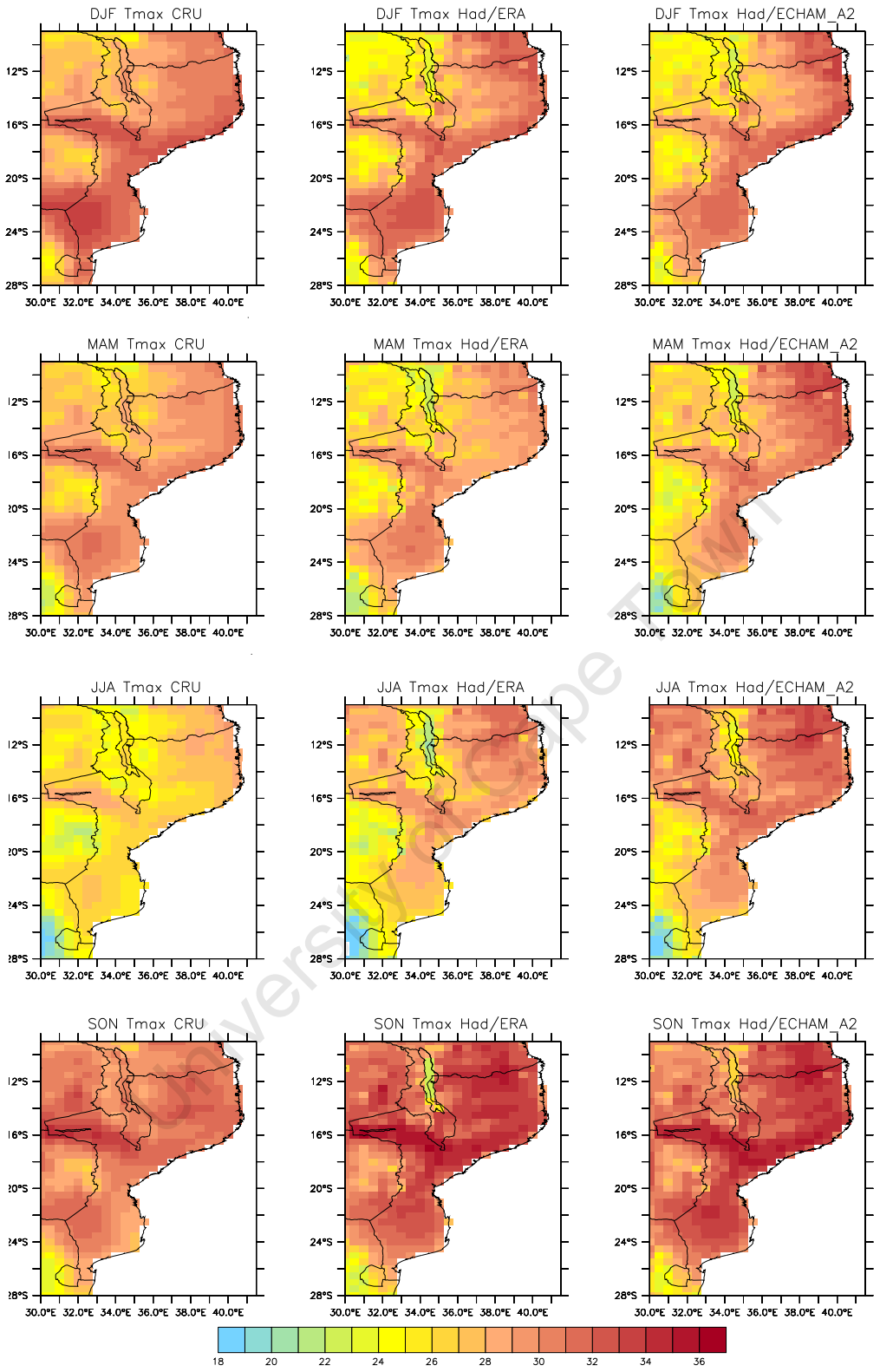

Figure 4.1: Climatological maximum temperature (°C) for the period 1981-1999 from the observations (CRU, *left*), Had/ERA (*centre*) and Had/ECHAM_A2 (*right*) for austral summer (*DJF*), austral autumn (*MAM*), austral winter (*JJA*) and austral spring (*SON*), respectively.

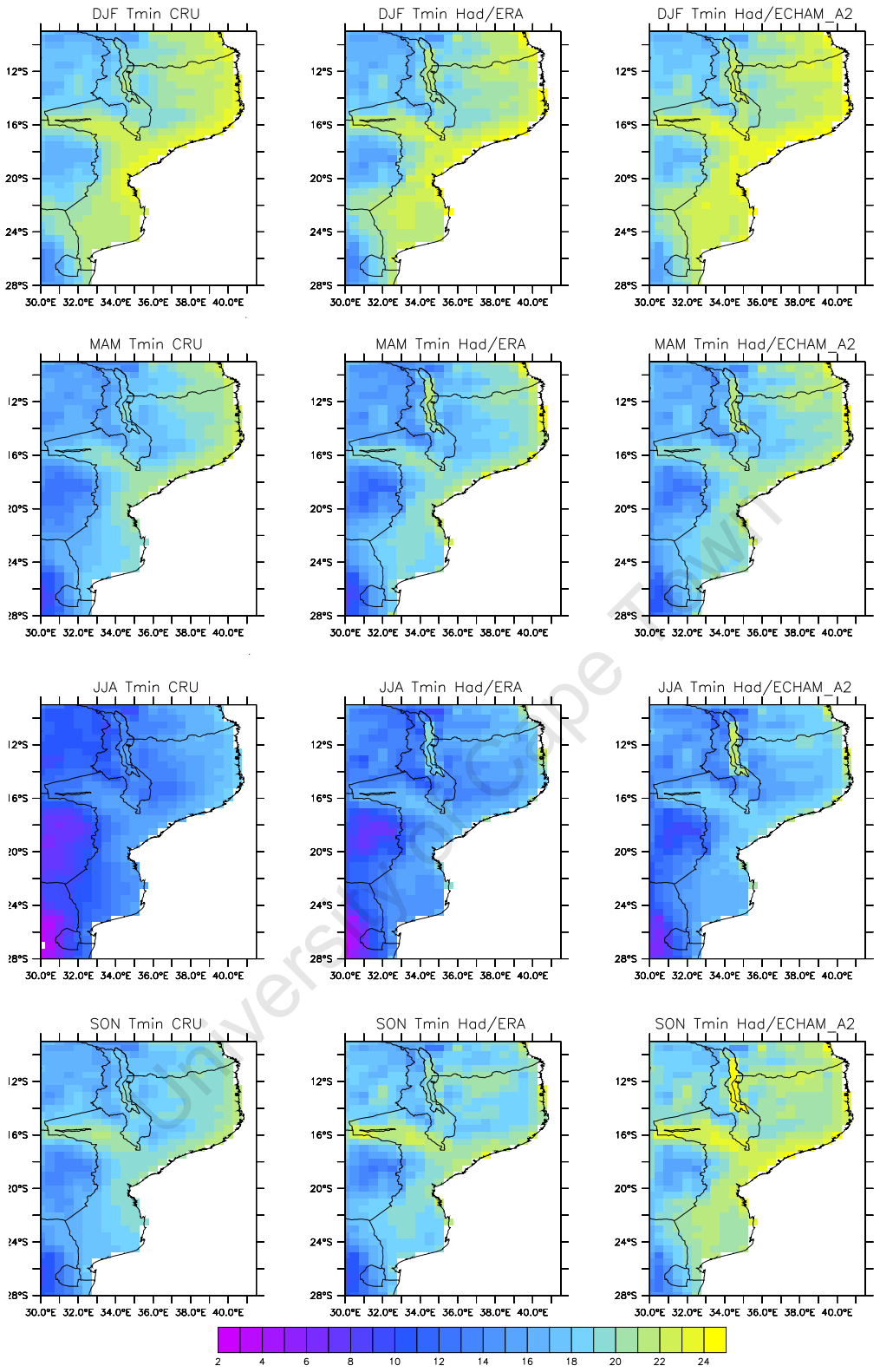

Figure 4.2: Climatological minimum temperature (°C) for the period 1981-1999 from the observations (CRU, *left*), Had/ERA (*centre*) and Had/ECHAM_A2 (*right*) for austral summer (*DJF*), austral autumn (*MAM*), austral winter (*JJA*) and austral spring (*SON*), respectively.

Maps of mean seasonal precipitation as simulated by Had/ERA and Had/ECHAM_A2 in comparison with that derived from the CRU observational data are shown in figure 4.3. During summer (DJF) both Had/ERA and Had/ECHAM_A2 reproduce the broad spatial distribution of precipitation (maximum in the north), however differences in magnitude are apparent. Had/ERA reproduces precipitation in excess over the coastal region of Zambezia during DJF. In summer the coast of Mozambique is affected by tropical cyclones, with between six and twelve storms per year occurring over the SW Indian Ocean, and about one to five passing south between Madagascar and the continent (Tyson and Preston-White, 2000). It is possible that in Had/ERA there is improved resolution of these storms, causing them to be more intense and/or persistent. These storms are associated with heavy rainfall. Also Had/ECHAM_A2 produces precipitation in excess of the CRU over Swaziland and over the Chimanimani mountains on the Zimbabwe border, which may be associated with orographic precipitation issues in the RCM. These increases in precipitation over the mountains are largely due to the finer resolution of the RCM causing enhanced topographical forcing and dynamical uplift.

During winter season (JJA) dry conditions over the region are well captured by both Had/ERA and Had/ECHAM_A2. During spring (SON) both simulations produce precipitation in excess of CRU observations. In the north, the summertime rainfall is mostly of convective origin associated by a complex interplay of converging airstreams which produce the Inter Tropical Convergence Zone (ITCZ). The two primary converging airstreams over East Africa are the north-east airflow from the East African monsoon, which crosses the equator and moves into eastern Africa, and south easterly trade winds off the Indian Ocean. Where these two airstreams meet a convergence zone, known as the ITCZ, is formed facilitating vertical motion. The misrepresentation of the position of the ITCZ over northern Mozambique in the regional model, largely determined by the forcing at the boundaries, affects the moisture advection and, in consequence, rainfall is underestimated over the region. Such complex system, is a difficult task to any climate model to accurately simulate. Besides this, rainfall may be underestimated also due to the deficiency of the convective scheme. This can explain why Had/ERA and Had/ECHAM_A2 underestimate the summertime rainfall in the north. For instance, Hein-Griggs (2008) found that HadRM3P represents extreme precipitation better in areas which large scale precipitation dominates than in areas in which convective rainfall dominates.

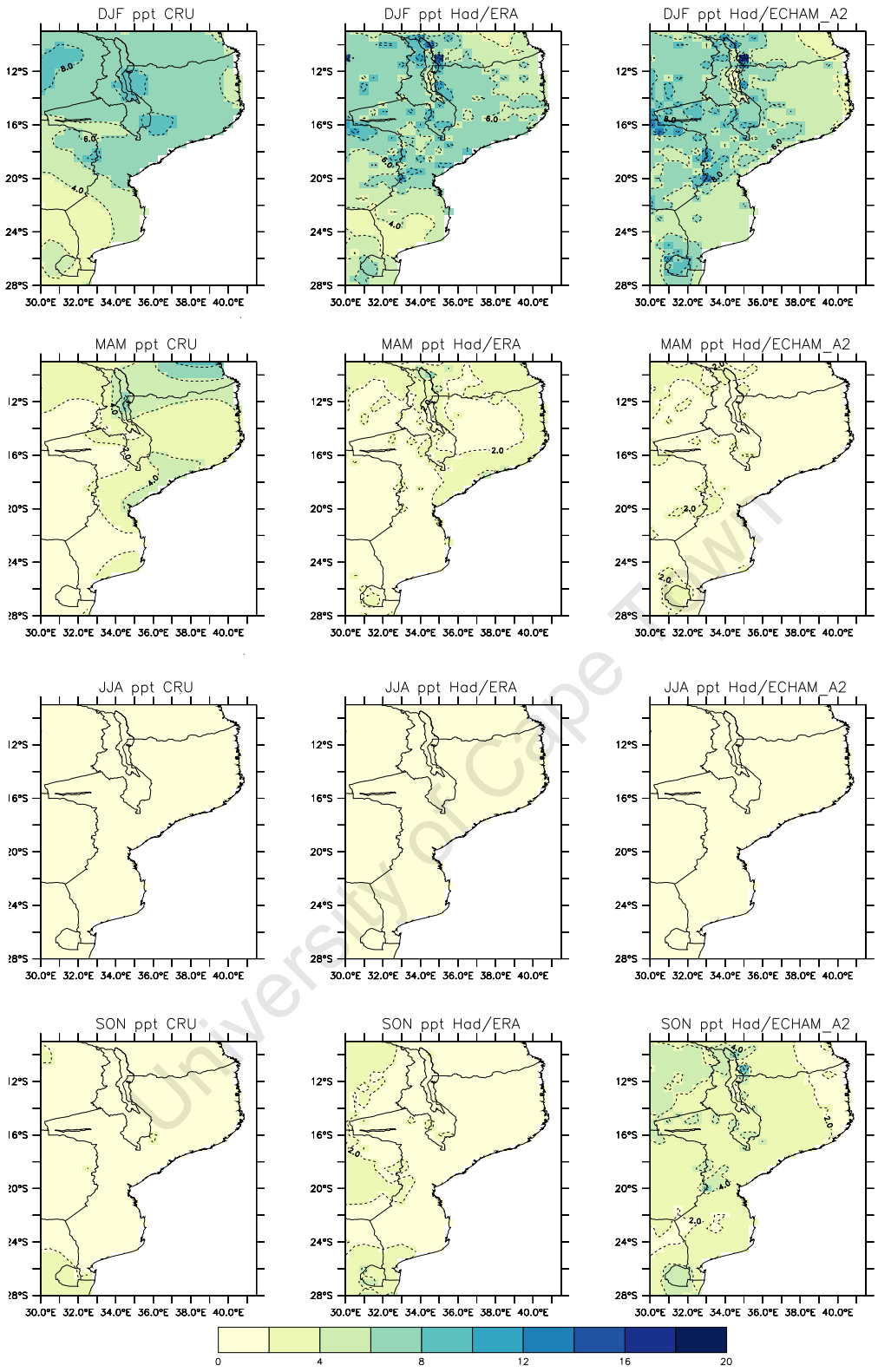

Figure 4.3: Climatological precipitation (mm/day) for the period 1981-1999 from the observations (CRU, *left*), Had/ERA (*centre*) and Had/ECHAM_A2 (*right*) for austral summer (*DJF*), austral autumn (*MAM*), austral winter (*JJA*) and austral spring (*SON*), respectively.

4.1.1 Comparison of Had/ERA with CRU

The model biases in reproducing the climatological fields are highlighted in figure 4.4. Model biases are calculated with respect to the observation dataset produced by the Climatic Research Unit (CRU) of the University of East Anglia (New et al., 1999, 2000). The model output was interpolated on the same common 0.5° grid. Model bias were calculated for each season for the reference 19 year period of 1981-1999, i.e. the model bias is defined as the difference between simulated (Had/ERA) and observed (CRU) (equation 3.1).

In general, Had/ERA appears characterized by a predominant cold bias of a few degrees in DJF and MAM, a predominant warm bias in JJA. One of the most pronounced features in the seasonal maximum temperature (T_{max}) and minimum temperature (T_{min}) maps is a very marked dominance of warm bias in JJA, where a bias of 5°C occurs at several regions. The warm bias found in JJA is likely due to less total cloud amount simulated from HadRM3P compared to total cloud amount from CRU climatology (Fig A.1 - see appendix A), as well as increasing in solar radiation heating (due to less cloud cover). This bias also might be associated with absence of precipitation during JJA, which tends to result in a decrease in soil moisture and latent heat flux, and as a result surface warming (e.g. Moberg and Jones, 2004). The cold bias is observed in the west over mountainous regions during DJF and MAM. This is a common feature of regional climate simulations over different regions of the world (Solman et al., 2008; Giorgi et al., 2004). The cold bias observed in T_{max} is generally between -1 and -4°C during DJF and MAM. However, during SON the country is dominated by a warm bias over the coast and north in T_{max} between 1 and 4°C. The model representation of T_{min} for many locations in the country is good, although a few locations with cold/warm bias (2°C) occur.

Regarding precipitation, the model presents a dry bias between 1 and 3 mm/day in the north of the country during DJF. During MAM a dry bias between 1 and 2 mm/day is found in some locations in the country and a dry bias up to 8 mm/day over Tanzania. A wet bias is observed over the mountain regions of Tete (2 mm/day) and Manica (3 mm/day) during SON

.

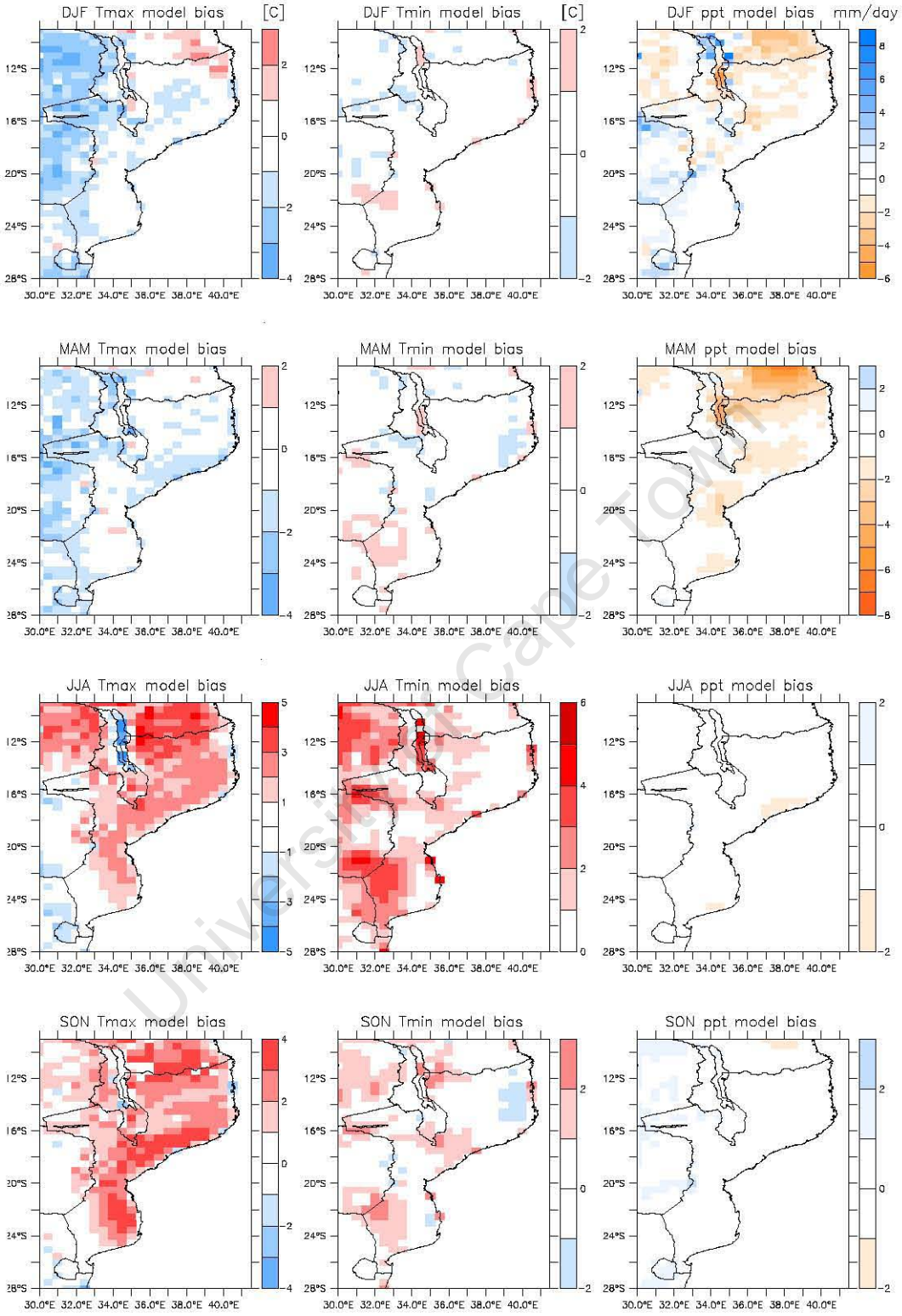

Figure 4.4: Model bias (Had/ERA-CRU) for T_{max} (*left*), T_{min} (*centre*) and *ppt* (*right*) for austral summer (*DJF*), austral autumn (*MAM*), austral winter (*JJA*) and austral spring (*SON*), respectively.

4.1.2 Comparison of Had/ECHAM_A2 with Had/ERA

Errors in HadRM3P can arise either from the internal RCM physics or from lateral boundary (LB) forcing, in this case the ECHAM4/OPYC3, that can introduce systematic biases in the simulation (Noguer et al., 1998). Figure 4.5 shows the bias ascribed to errors inherited from the forcing ECHAM4/OPYC3 through the lateral boundary condition (LBC). The bias is defined as the difference between the RCM forced by ECHAM4/OPYC3 GCM and the RCM forced by ERA40 (equation 3.2).

During DJF the cold bias is increased between 1 to 2°C over Limpopo Basin in maximum temperature (T_{max}). During all seasons except DJF, the country is characterized by a warm bias, however the bias is higher during JJA and SON. During JJA the warm bias in T_{max} and T_{min} is exacerbated by the forcing ECHAM4/OPYC3.

Regarding to rainfall the LBC introduces a localized dry bias in the simulations in some regions in the cost and wet bias in the interior. Except during SON when the LBC intruduce a wet bias. The lateral boundary forcing reduces precipitation over Zambézia. Since the biases are present in both Had/ECHAM_A2 and Had/ERA, some of these biases are not only due to errors in the internal model physics of HadRM3P, but also to the effects of lateral boundary conditions.

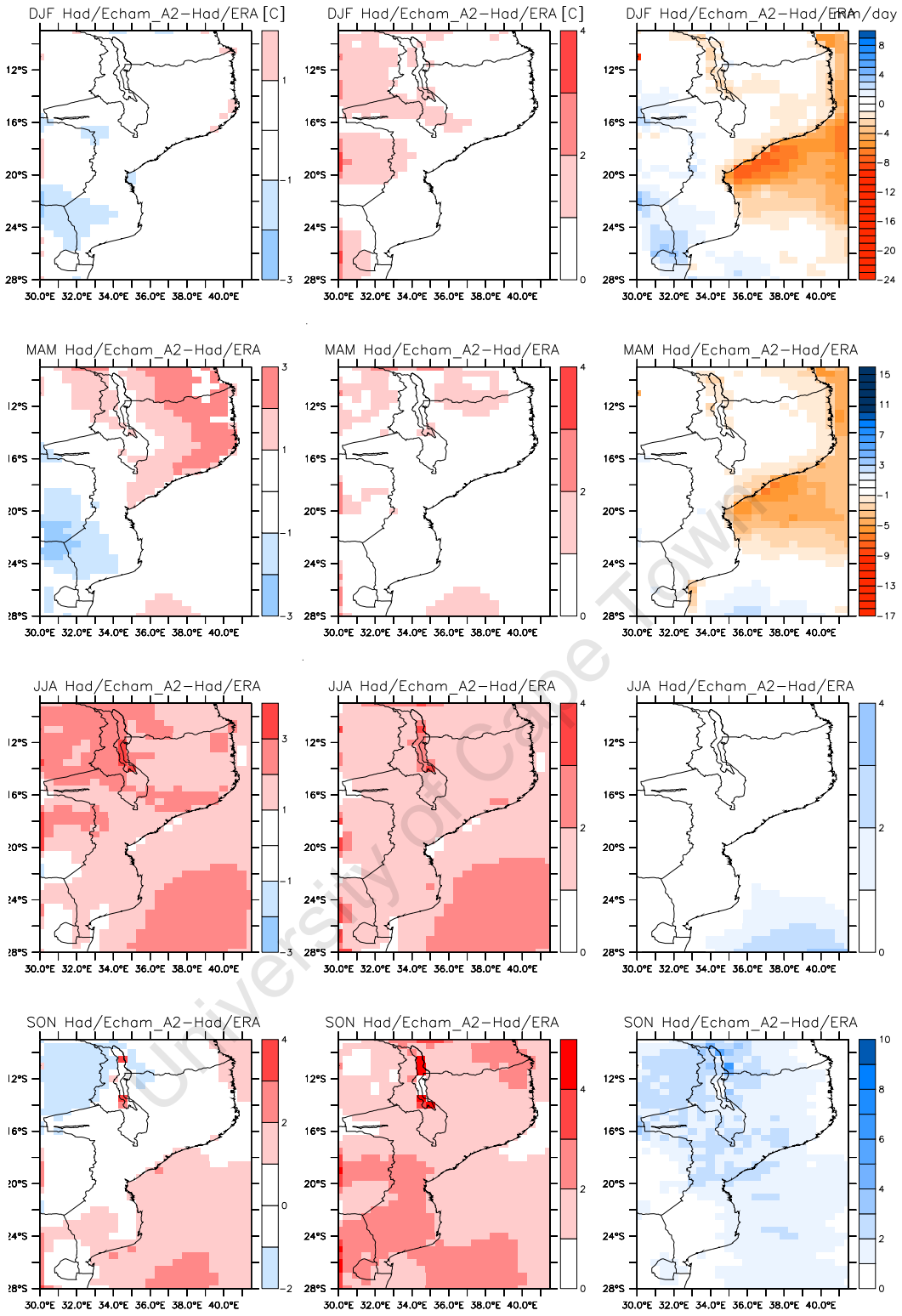

Figure 4.5: Echam bias (Had/ECHAM_A2-Had/ERA) for T_{max} (*left*), T_{min} (*centre*) and *ppt* (*right*) for austral summer (*DJF*), austral autumn (*MAM*), austral winter (*JJA*) and austral spring (*SON*), respectively.

4.1.3 Comparison of modeled daily frequencies with observations

Model daily output (Had/ERA and Had/ECHAM_A2) is also validated against daily observed data of 32 stations over Mozambique. A PDF of stations and model daily output data from the present climate (1981-1999) is shown in figure 4.6. The modeled PDFs are constructed considering only points over Mozambique (figure A.2) to explore the capacity of the model in simulate the PDFs of maximum temperature (T_{max}), minimum temperature (T_{min}), and precipitation (ppt). The PDFs are described using the empirical distribution moments.

Figure 4.6 (a) and (b) presents the PDFs of observed and modeled T_{max} and T_{min} for Mozambique. The shape of T_{max} is captured well by Had/ERA and Had/ECHAM_A2, with a slight overestimation of the right tail of the PDF (i.e. the hot extremes) and underestimation of the left tail (i.e. the cold extremes) in the model data. Both Had/ERA and Had/ECHAM_A2 simulations underestimate the most probable maximum temperatures, with ECHAM4/OPYC3 boundary conditions making little difference to the model simulations. Minimum temperature is largely overestimated and the curve is highly skewed whereas the station curve is wider and less skewed to higher temperatures. There is a tendency of Had/ERA and Had/ECHAM_A2 to underestimate the probability of lower minimum temperatures but overestimate the probability of warmer minimum temperatures. Had/ECHAM_A2 simulates notably higher minimum temperatures than Had/ERA.

Figure 4.6 (c) shows the PDFs for ppt. Had/ERA and Had/ECHAM_A2 overestimate the number of light precipitation events (< 14 mm day^{-1}) and underestimate the number of heavier precipitation events i.e > 14 mm day^{-1}. One reason to this result is that the density of stations in the observed dataset is insufficient to capture large area (e.g. 0.22 degree gridsquare) low precipitation events.

Table 4.1 shows the upper (Tx90p an Tn90p) and lower (Tx10p and Tn10p) percentile of T_{max} and T_{min}, and precipitation indices (R95p and R99p). In general, temperature indices are well reproduced by Had/ECHAM_A2 and Had/ERA when compared with precipitation indices.

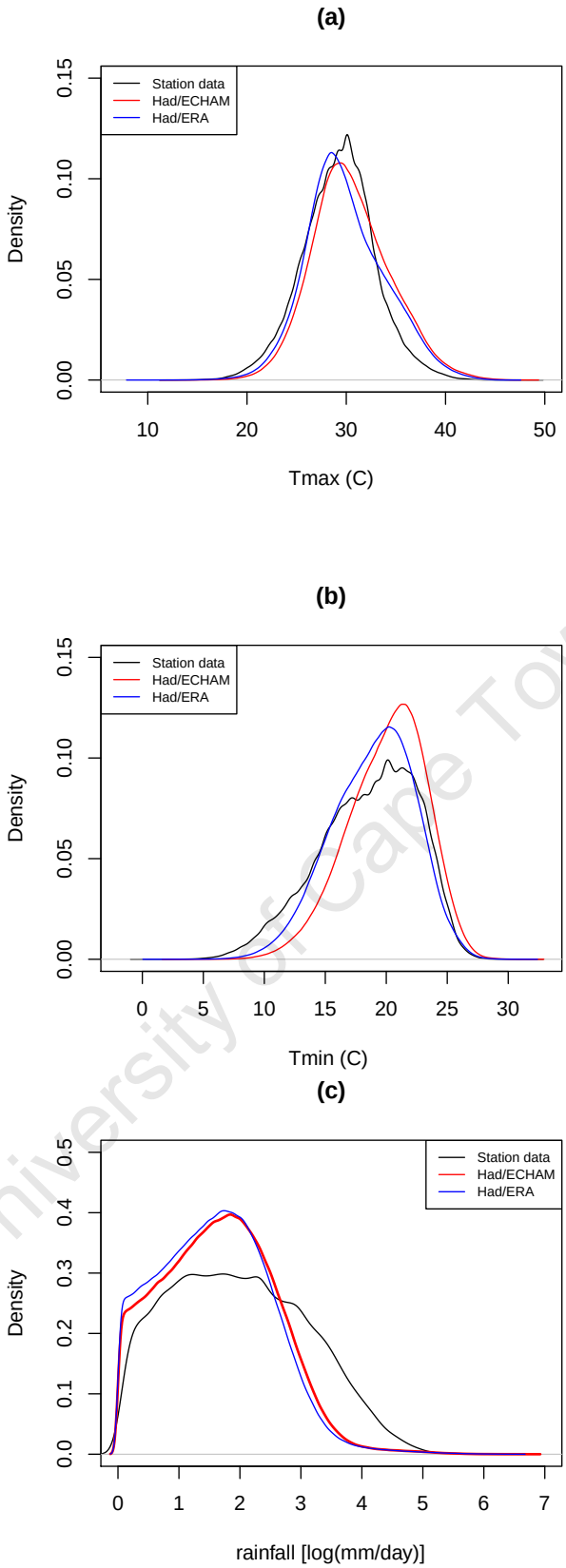

Figure 4.6: Comparison of probability density functions of daily T_{max} (a), T_{min} (b), and daily precipitation (c) observations in 32 stations whith Had/ERA and Had/ECHAM_A2 simulations over Mozambique during 1981-1999.

Table 4.1: Percentiles of daily T_{max}, T_{min} (in °C) and daily precipitation (in mm day^{-1}) from observed and modeled data. The percentiles were calculated for the period 1981 to 1999.

	Tx10p	Tx90p	Tn10p	Tn90p	R95p	R99p
Station data	24.6	33.7	13.0	23.4	49.2	90.7
Had/ECHAM_A2	25.7	36.0	15.7	24.0	23.2	50.0
Had/ERA	25.2	35.6	14.3	23.1	21.2	48.6

The ability of the regional model to represent the observed Mozambican climate was assessed to support confidence in the results. Particular attention was devoted to the validation of temperature and precipitation, since these are such important variable for human impacts. Precipitation is one of the more difficult variables to be simulated by the models due to its greater variability, both in time and space. The present simulation (Had/ERA) performs quite well in terms of temperature during the 19 years of validation except during JJA where Had/ERA overestimate the temperature. For precipitation the present simulations also performs reasonable well, however some biases exists. With ECHAM4/OYPC3 forcing (Had/ECHAM_A2) an opposite bias to that of the Had/ERA was found. In some seasons the bias was exacerbated (e.g. during JJA) while in others the bias was diminished (during DJF but for T_{max}); this illustrates the impacts of the boundary conditions on the regional simulations. The magnitude of the biases found in this study are similar in others regional climate simulations (e.g. Hudson and Jones, 2002; Solman et al., 2008; Moberg and Jones, 2004). Analysis in more variables (e.g. soil moisture, related to circulation) would be necessary for a more complete understanding of the causes of temperature and precipitation biases. The main focus in the dissertation was to characterize details in how well the model temperature and precipitation represent the "reality". However, further model development for the region should be focused on physical parameterizations of various sub-scale processes. Despite the biases, in the opinion of the author the performance of the model (HadRM3P) over Mozambique is of sufficient quality for application to the study of climate change over Mozambique.

4.2 Future projection of extremes

Projections of future change of extreme events are assessed by analysing differences in the extreme indices (presented in table 3.1) of temperature and precipitation on a seasonal basis between present and future climate. The output from HadRM3P forced by ECHAM/OPYC3 under Special Report on Emissions Scenario (SRES) A2 scenario (Had/ECHAM_A2) is used. The model data is subdivided into three subsamples: the 1981-1999, 2011-2029 and the 2031-2049 periods, defining the control (CTL), middle (MDL) and future (SCN) climate, respectively.

4.2.1 Changes in the PDFs

The Probability density functions (PDF) of daily values of maximum temperature (T_{max}), minimum temperature (T_{min}) and precipitation (ppt) over the selected regions (figure 3.2) are analysed for present climate (1981-1999, CTL), middle (2011-2029, MDL) and future scenario (2031-2049, SCN) for the four seasons (DJF: December to February, MAM: March to May, JJA: June to August and SON: September to November). The PDFs represents the probability of occurrence of a given temperature and/or precipitation amount over the selected regions (not in a single model grid cell) also integrated in time.

Figures 4.7 and 4.8 shows the daily probability distribution function (PDF) of maximum and minimum temperature for DJF and JJA, respectively. Regions 1 to region 4 are situated along the coast and regions 5-8 are situated in the interior. In the coastal regions, the PDFs of T_{max} and T_{min} have two marked maxima. This bimodality is likely due to the temperature difference between land and sea. The distribution of T_{max} and T_{min} show a clear shift to warmer values in a future climate for all regions presented. This shift of the distribution to higher values in the future implies that there will be an increase in extreme events associated with the hotter tail of the distribution and a decrease in extreme events associated with the colder tails. The shape of the distribution (unimodal/bimodal) is maintained across all regions.

Table 4.2 and 4.3 summarize the changes in upper and lower percentile changes in maximum and minimum temperature for each of the four seasons for the two periods MDL and SCN. During summer (DJF), changes in 10^{th} percentile of maximum temperatures (Tx10p

- cold days) and 90^{th} percentile of maximum temperatures (Tx90p - warm days) are projected to increase in all regions, with changes in Tx90p (of the order of 1.3°C in region 3 to 2.1°C in region 8) being greater than changes in Tx10p (1°C in region 3 to 1.5°C in region 7). During winter (JJA) changes in 10^{th} percentile of minimum temperatures (Tn10p - cold nights) and 90^{th} percentile of minimum temperatures (Tn90p - warm nights) are also projected to increase in the future in all regions. However, changes in Tn10p are projected to be greater in coastal regions than that of Tn90p for the same regions. In regions in the interior, the change in Tn10p and Tn90p have the same magnitude (1.3°C), excepted for the region 5 where change in Tn90p is greater than Tn10p. During late summer (MAM) changes in Tx90p are projected to decrease (-0.6 to -0.1°C) over the regions 2, 3, 6 and 7 for the MDL period. The highest changes in Tx10p and Tx90p are found particularly during the early summer (SON). Similar results are also found for Tn10p and T90p. In general changes in extreme temperature indices are higher at regions in the interior and lower at coastal regions partly due to the influence of the ocean. These findings suggest that these eight regions will experience extreme hot events of greater magnitude and less extreme cold events especially during the late summer season (SON) before the onset of the rains over much of the country.

Figure 4.9 shows the PDF of precipitation intensity during summer when most precipi-

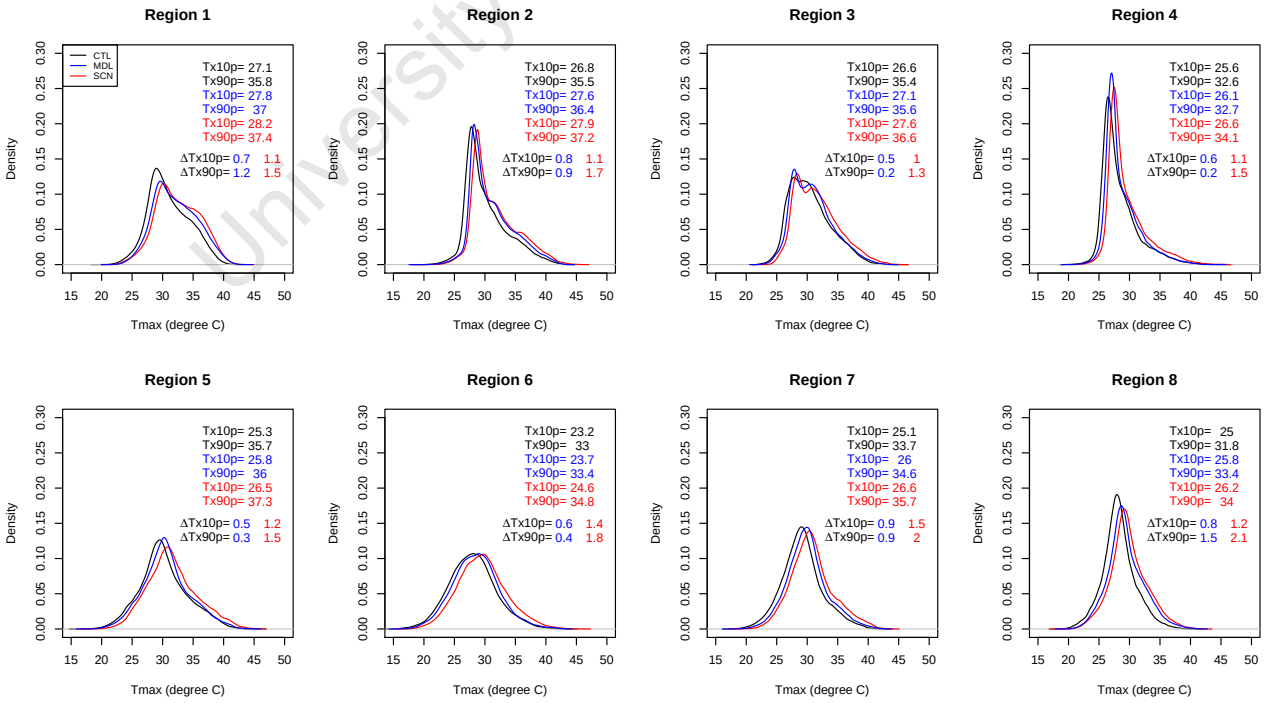

Figure 4.7: Daily maximum temperature probability distribution function for DJF in CTL (1981-1999, black), MDL(2011-2029, blue) and SCN (2031-2049, red) simulations

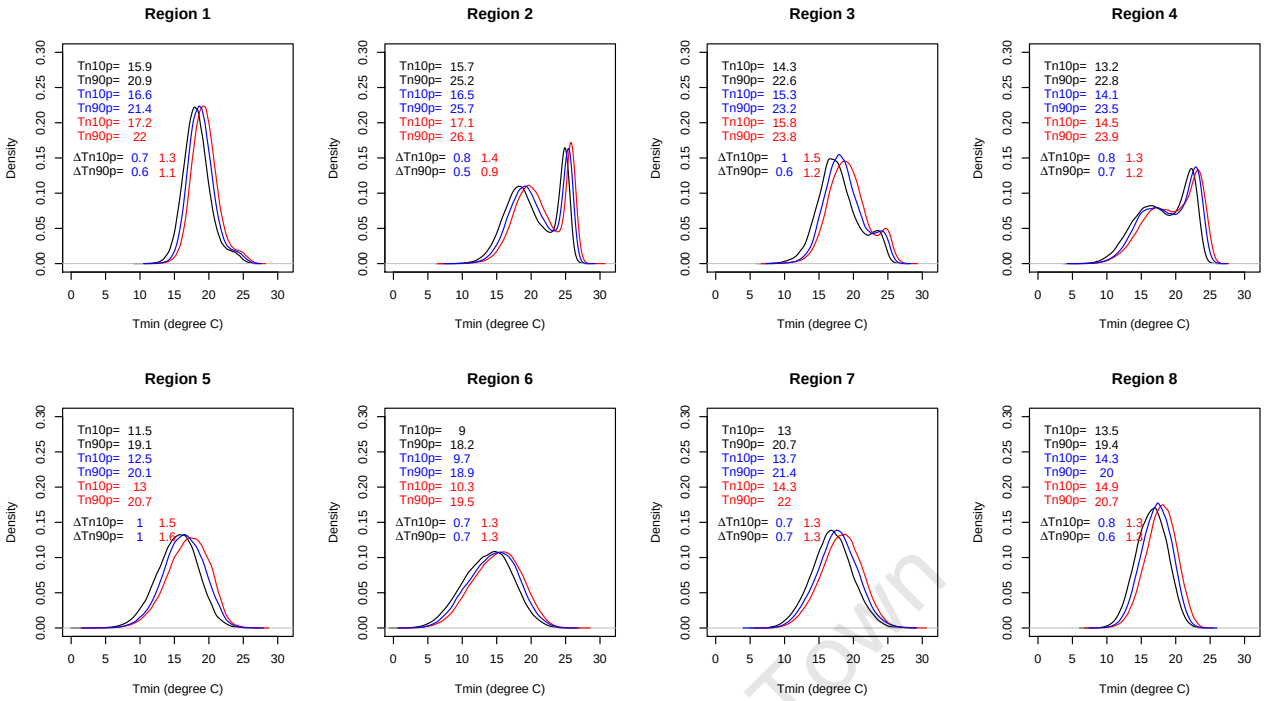

Figure 4.8: Daily minimum temperature probability distribution function for JJA in CTL (1981-1999, black), MDL(2011-2029,blue) and SCN (2031-2049, red)

tation and extreme events typically occur (Tyson and Preston-White, 2000). The PDFs of precipitation intensity for other seasons are shown in appendix. The PDF for DJF exhibits a shift toward higher precipitation intensities in SCN, but many values overlap with MDL and CTL values, indicating relatively small changes. Table 4.4 presents the changes in percentage of the precipitation indices for each of the four seasons for both periods analysed. Changes in projected precipitation indices R95p and R99p, are much more heterogeneous than for temperature indices. During summer the changes in R95p and R99p are projected to decrease in region 4 from MDL through SCN by 8.3% and 20.9%, respectively. However, the changes over other regions are projected to increase with region 2 having the highest change during MDL and SCN in both R95p and R99p. These increases of extreme precipitation in the region might be associated with tropical cyclone activity in the immediate vicinity of the region during summer. This hypothesis that cyclone activity contribute for extreme precipitation over the coastal regions will be tested in the near future research. During late summer (MAM) the changes in R95p and R99p are higher in region 2 during MDL compared to other regions. In contrary to other regions, the changes in R95p are projected to decrease from MDL (10.8%) to SCN (1.4%) in region 5. During early summer (SON) a projected decrease in precipitation indices (R95p and R99p) are found in region 1, 2 and 3

during MDL. In contrast, during SCN these indices are projected to increase over the same regions. These increasing changes in R95p and R99p suggest more likely extreme events in the future (SCN).

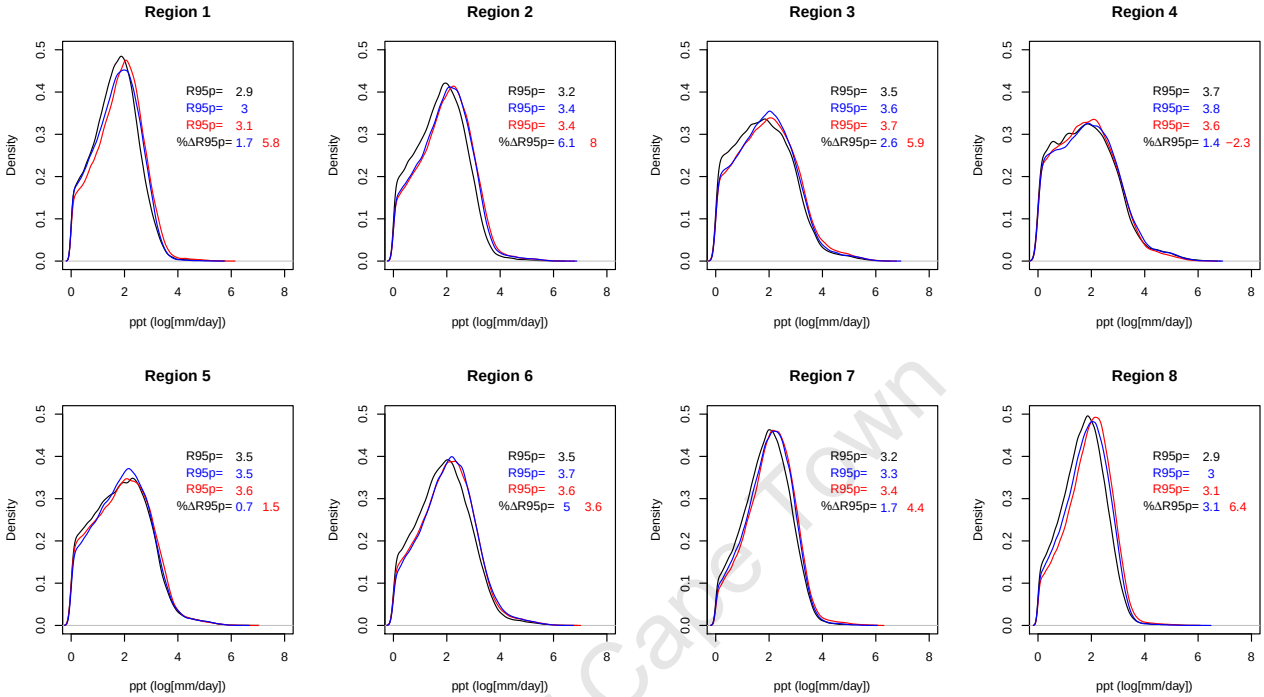

Figure 4.9: Daily total precipitation probability distribution function for DJF in CTL (1981-1999, black), MDL (2011-2029, blue) and SCN (2031-2049, red) simulations

Table 4.2: Changes (°C) in Tx10p and Tx90p between MDL-CTL and SCN-CTL

	DJF				MAM				JJA				SON			
	MDL-CTL		SCN-CTL		MDL-CTL		SCN-CTL		MDL-CTL		SCN-CTL		MDL-CTL		SCN-CTL	
	△Tx10p	△Tx90p	△Tx10p	△Tx90p	△Tx10p	△Tx90p	△Tx10p	△Tx90p	△Tx10p	△Tx90p	△Tx10p	△Tx90p	△Tx10p	△Tx90p	△Tx10p	△Tx90p
Region 1	0.7	1.2	1.1	1.5	0.7	0.2	1.2	0.8	0.5	0.4	1.0	0.9	0.9	0.6	1.9	1.6
Region 2	0.8	0.9	1.1	1.7	0.5	-0.6	1.0	0.9	0.5	0.6	1.0	1.2	0.7	1.1	1.2	2.5
Region 3	0.5	0.2	1.0	1.3	0.5	-0.1	0.9	0.7	0.6	0.7	1.1	1.4	0.9	1.0	1.5	2.6
Region 4	0.6	0.2	1.1	1.5	0.5	0.4	0.9	1.4	0.6	0.6	0.9	1.3	0.9	1.6	1.3	2.9
Region 5	0.5	0.3	1.2	1.5	0.5	0.4	1.2	1.4	0.9	0.7	1.4	1.5	1.2	1.3	2.0	2.9
Region 6	0.6	0.4	1.4	1.8	0.5	-0.4	1.2	0.8	0.3	0.5	0.9	1.2	1.2	1.2	2.1	2.8
Region 7	0.9	0.9	1.5	2.0	0.2	-0.6	0.9	0.8	0.4	0.6	0.9	1.2	1.7	1.1	2.7	2.5
Region 8	0.8	1.5	1.2	2.1	0.4	0.2	1.3	1.0	0.4	0.5	0.9	1.1	1.4	0.8	2.4	1.9

Table 4.3: Changes (°C) in Tn10p and Tn90p between MDL-CTL and SCN-CTL

	DJF				MAM				JJA				SON			
	MDL-CTL		SCN-CTL		MDL-CTL		SCN-CTL		MDL-CTL		SCN-CTL		MDL-CTL		SCN-CTL	
	△Tn10p	△Tn90p	△Tn10p	△Tn90p	△Tn10p	△Tn90p	△Tn10p	△Tn90p	△Tn10p	△Tn90p	△Tn10p	△Tn90p	△Tn10p	△Tn90p	△Tn10p	△Tn90p
Region 1	1.0	0.9	1.5	1.4	0.9	0.7	1.4	1.3	0.7	0.6	1.3	1.1	0.8	0.7	1.3	1.3
Region 2	1.4	0.6	1.9	1.0	0.9	0.4	1.4	0.9	0.8	0.5	1.4	0.9	1.0	0.7	1.8	1.5
Region 3	1.7	0.7	2.0	1.2	0.6	0.4	1.3	1.2	1.0	0.6	1.5	1.2	1.1	0.9	1.6	1.6
Region 4	1.2	0.5	1.9	1.0	0.7	0.5	1.4	1.0	0.8	0.7	1.3	1.2	1.2	0.9	1.7	1.7
Region 5	1.4	0.8	1.9	1.3	0.7	0.5	1.5	1.4	1.0	1.0	1.5	1.6	1.0	1.2	1.7	2.2
Region 6	1.3	1.0	1.7	1.5	1.1	0.6	1.7	1.3	0.7	0.7	1.3	1.3	0.9	1.2	1.6	2.1
Region 7	1.2	1.0	1.8	1.5	0.8	0.5	1.5	1.3	0.7	0.7	1.3	1.3	1.0	1.3	1.8	2.6
Region 8	1.2	0.9	1.7	1.5	1.0	0.8	1.6	1.4	0.8	0.6	1.3	1.3	1.0	0.8	1.6	1.8

Table 4.4: Percent change of R95p and R99p

	DJF				MAM				JJA				SON			
	MDL-CTL		SCN-CTL		MDL-CTL		SCN-CTL		MDL-CTL		SCN-CTL		MDL-CTL		SCN-CTL	
	△R95p	△R99p	△R95p	△R99p	△R95p	△R99p	△R95p	△R99p	△R95p	△R99p	△R95p	△R99p	△R95p	△R99p	△R95p	△R99p
Region 1	5.2	-3.0	18.5	23.2	8.6	3.8	17.9	6.5	-9.1	-1.0	-18.6	-11.7	-5.0	-5.0	8.5	16.3
Region 2	21.2	60.0	28.7	59.5	26.2	39.5	13.8	27.3	0.3	-3.4	-3.5	5.7	-5.3	-7.9	9.7	16.9
Region 3	9.5	16.9	23.2	26.4	6.4	23.4	9.8	20.8	-4.4	1.1	2.9	10.2	-15.0	-28.7	-1.0	-9.4
Region 4	5.2	-0.9	-8.3	-20.9	5.2	1.2	10.2	15.1	-6.9	-6.6	2.9	-1.5	21.3	19.3	11.9	2.7
Region 5	2.6	-1.6	5.6	-2.2	-10.8	-9.7	-1.4	13.4	6.9	-18.1	34.6	0.5	-5.8	-13.8	-0.9	11.3
Region 6	19.2	25.1	13.4	27.8	14.3	23.8	11.3	3.2	14.9	28.7	10.7	9.3	-3.5	-14.5	9.1	15.3
Region 7	5.7	7.5	15.1	50.9	17.9	14.9	12.0	8.1	10.0	16.4	59.2	115.9	1.5	-4.1	9.4	20.7
Region 8	9.4	1.8	20.8	23.7	19.4	13.1	22.7	17.0	18.3	-13.3	15.5	-10.2	0.5	-3.1	13.4	26.5

4.2.2 Spatial changes of upper and lower percentiles

The spatial changes in the intensity of the extreme are presented here. As a measure of intensity of extreme temperature conditions, the 10^{th} and 90^{th} percentile changes in maximum and minimum temperature of daily data corresponding to all seasons for 19 years model period are depicted in figure 4.10. The results show that the increase in extreme temperature not only varies by region, but also between seasons.

The intensity of the 10^{th} and 90^{th} of the maximum and minimum daily temperature in all seasons increases from the control to the scenario period in all areas of the country. These changes are, however, not the same in every season: in SON the Tx10p shows increase (3-4°C) in the North with the same magnitude of increase in Tx90p over central and south. The increase of Tn10p is higher compared to Tx10p except during SON.

Change in Tx90p is higher in summer than winter everywhere in the country whereas in case of Tx10p, the change is higher in winter over the South (Gaza and Inhambane provinces) and central part of Mozambique (particularly along the coast of Zambézia province). Change in Tn10p is higher in summer over the country. The upper threshold of minimum temperature (Tn90p) shows larger change over Southern areas of Mozambique (Gaza and Maputo provinces). On the whole, increases are larger in Tx90p and Tn10p. These changes suggest that the intensity of hot extremes will increase all over the country. On the other hand, intensity of cold extremes will decrease. This means that the tails of the distribution of maximum and minimum temperature will shift to a warmer climate.

Changes in the intensity of extremes are accompanied with changes in their frequency of occurrence. Figure 4.11 shows the changes (in percentage) in frequency of the 10^{th} and 90^{th} percentiles of daily maximum and minimum temperatures. In summer, the majority of the country will experience more often number of days with extreme low and high temperatures. The frequency of warm days (Txf90) will increase (6 to 10٪) especially over the coastal provinces and the frequency of cold nights (Tnf10) are projected to increase to 14٪. During MMA the changes in the frequency of extreme cold days (Txf10) are projected to increase (6 to 14٪) all over the country, while the number of extreme warm days are projected to decrease (6 to 10 ٪) in the south. The numbers of extreme cold nights are projected to increase

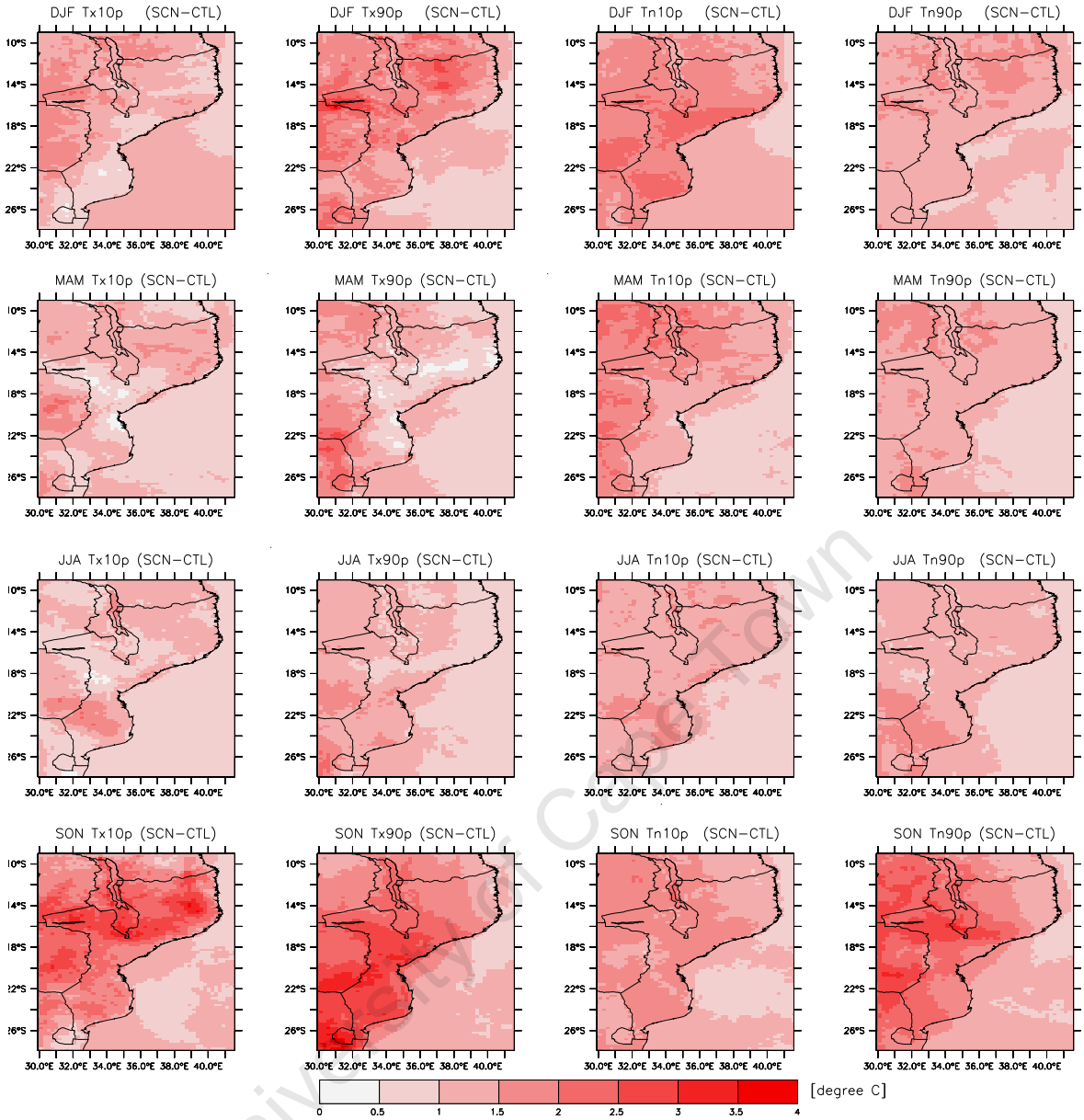

Figure 4.10: Changes in intensity of upper and lower percentiles temperature (SCN-CTL) for austral summer (*DJF*), austral autumn (*MAM*), austral winter (*JJA*) and austral spring (*SON*), respectively.

in the south while the number of extreme warm nights (Tnf90) decreases in the same region. The Tnf10 are also projected to increase in the south in winter while Txf90 decreases along the coast. In winter (JJA) the frequency of warm nights is projected to increases in most of the provinces with maximum change in 18% in Niassa province. However, the frequency of cold nights (warm nights) is projected to increase (decrease) in Gaza and Inhambane. During SON the frequency of cold days is projected to increase in the north (22% in Cabo Delgado province) with more frequency than in other seasons while the frequency of warm days will

increase/decrease less frequently compared to other seasons.

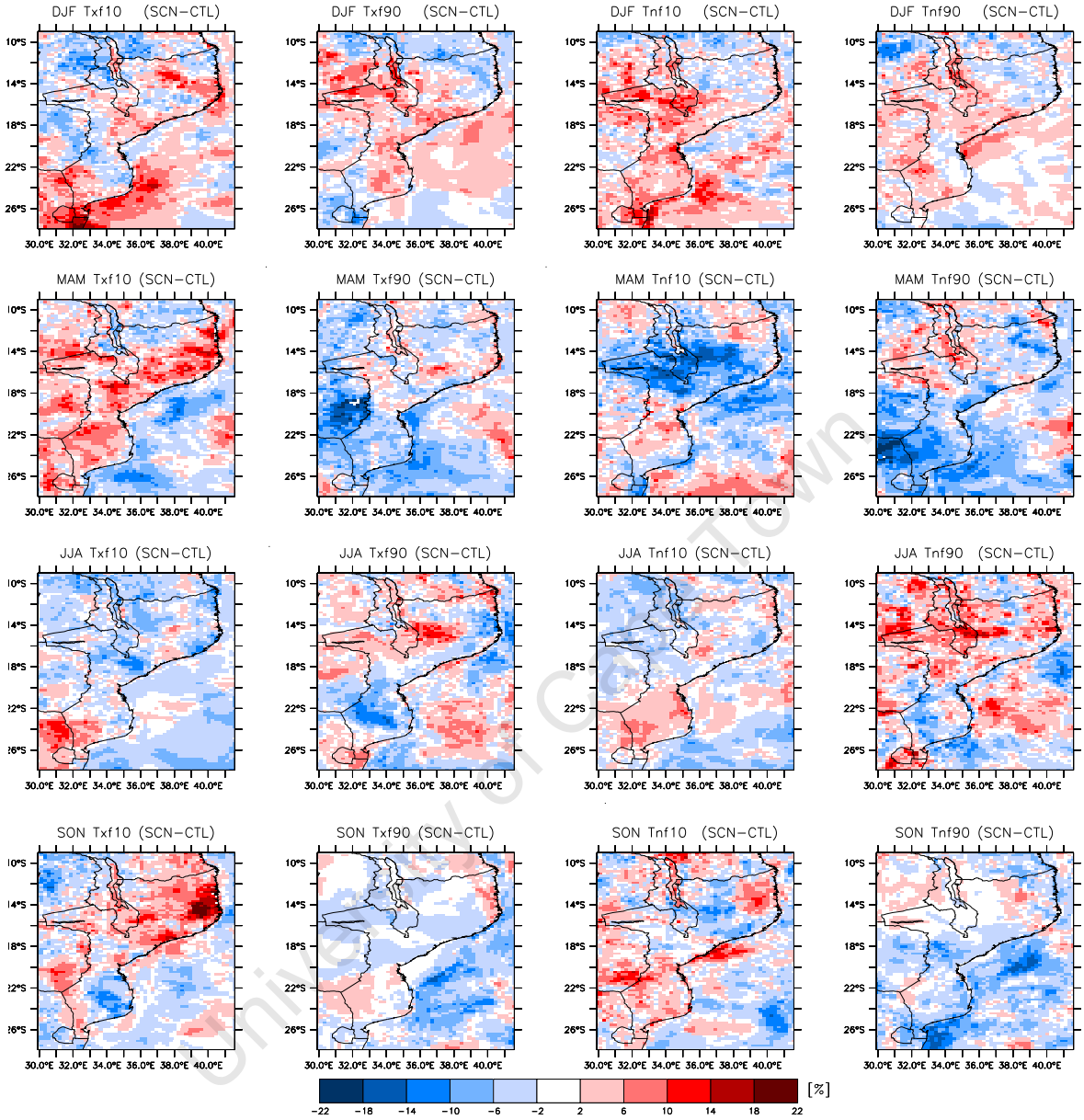

Figure 4.11: Changes in frequency of upper and lower percentiles temperature (SCN-CTL) for austral summer (*DJF*), austral autumn (*MAM*), austral winter (*JJA*) and austral spring (*SON*), respectively.

Figure 4.12 shows the changes in the indices R95p and R99p for three seasons (DJF, MAM and SON). These indices indicate the amount of precipitation during very wet days and extremely wet days. The measure of changes in the indices R95p and R99p are shown as percentage change

$$Change = 100 \times (\frac{scn}{ctl} - 1) \tag{4.1}$$

where *scn* and *ctl* are used to designate the indices in the future period and present period, respectively.

R95p is projected to increase in 30% for the most parts of the country during DJF. However, there are localized areas which will experience increments up to 70% (Sofala and Inhambane provinces). R99p are also projected to increase over most parts of the country, except on the south where it is observed a negative change (decrease). The largest positive change in R99p occurs in the centre of the country. In the south (Maputo province) the R99p is projected to decrease (30 to 70%). Positive changes of R95p and R99p in the centre will enhance the flooding risk, since this area is prone to floods. During MAM the R95p are projected to increase in many parts of the north and centre of Mozambique. Changes in R95p and R99p during SON are more heterogeneous than other seasons, with increases and decreases. Increases in extreme rainfall are higher during DJF compared to MAM and SON due to increases in surface heating and moisture.

Future change in R95p and R99p are accompanied by changes in consecutive number of dry days (CDD - defined as days with a total precipitation less than 1mm) and consecutive number of wet days (CWD - defined as days with a total precipitation of 1mm or more). Figure 4.13 shows the change in consecutive number of dry days and consecutive number of wet days for DJF, MAM and SON. During DJF, changes in CDD occur at localized regions over the country. In northeast (Cabo Delagado and Nampula) there are increases of CDD up to 15 days and a decrease in the west. While there are increases in CWD almost everywhere over the country, except in Cabo Delgado and in some localized regions in Tete where the CWD decreases. The increases in CWD together with extremes of precipitation suggest that during DJF the country will experience more days with intense extreme precipitation during the rainy season increasing the probabilities of floods over Zambeze basin. Increases in CDD during SON means that the onset of rain over much of the country will start late. This will have negative impacts in agriculture, since the agriculture in Mozambique is most dependent

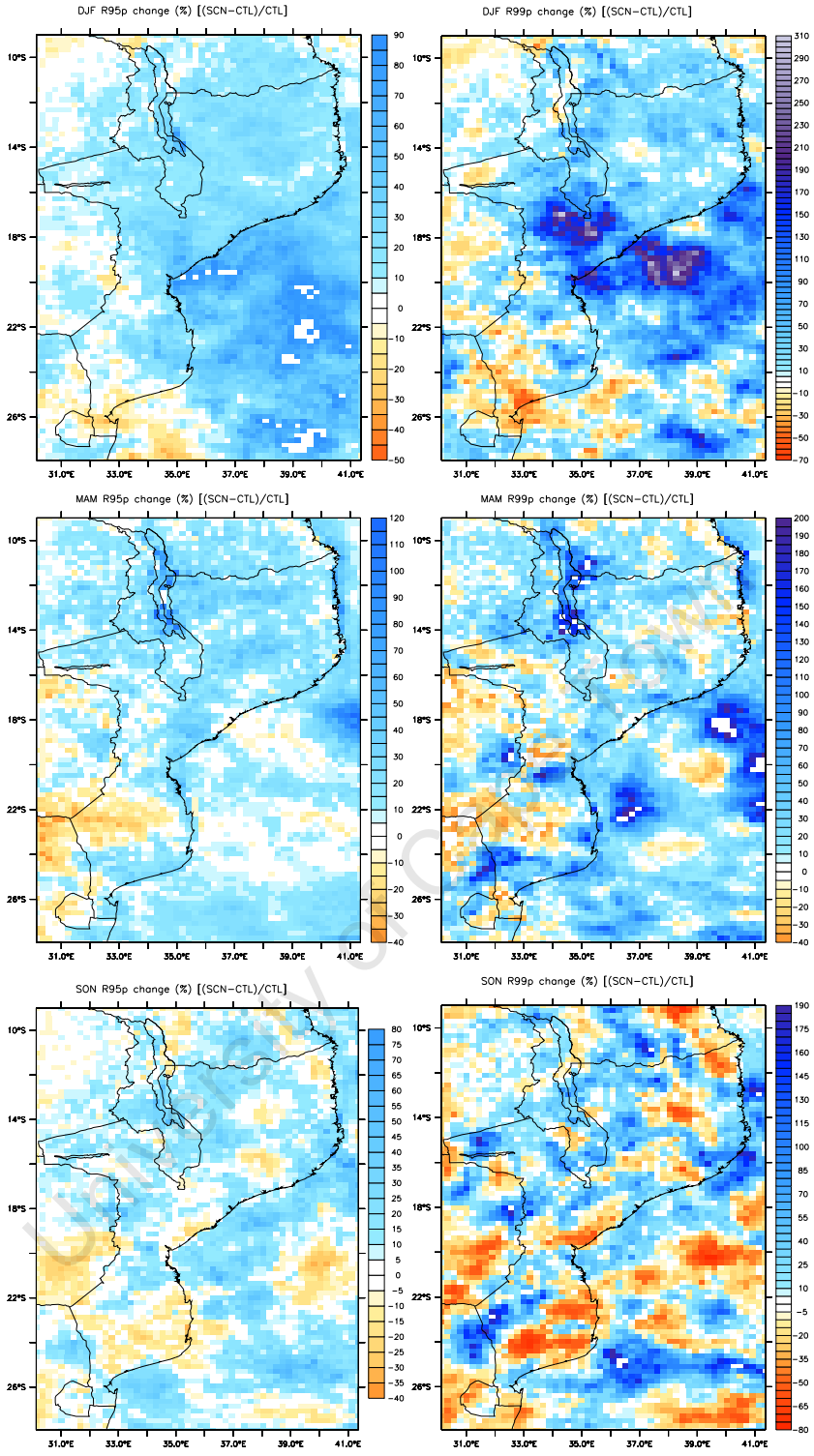

Figure 4.12: Projected changes (%) in 95th (*left*) and 99th (*right*) percentile of precipitation amount for DJF (*top*), MAM (*middle*) and SON (*bottom*). A minimum rainday threshold of 1 mm was used.

on rainfall.

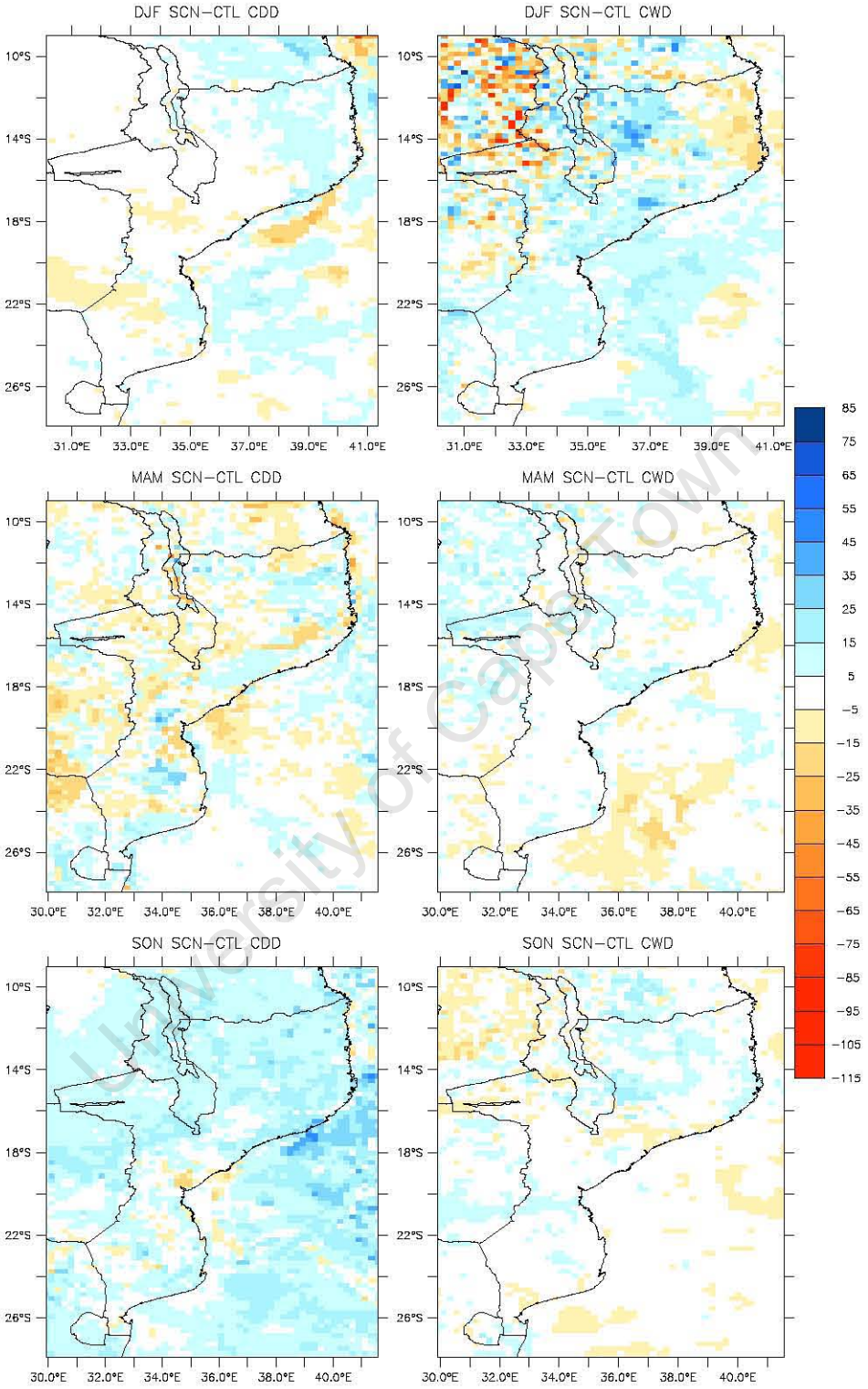

Figure 4.13: Change of maximum number of consecutive dry days (CDD, *left*) and consecutive wet days (CWD, *right*).

4.3 Dominant synoptic types

The basic aim of synoptic climatology is to relate local or regional climates to the large scale atmospheric circulation (Yarnal, 1993). This require classifying atmospheric circulation types and then relating a local variable (e.g. temperature, precipitation) to these circulation types. To investigate the favorable atmospheric circulation patterns that may explain some of the changes in extreme precipitation and extreme temperature mentioned in the previous sections, a general classification of daily 850 hPa geopotential height patterns for south east Africa was created using 7x5 nodes.

4.3.1 Simulated synoptic types

Figure 4.14 shows the SOM general classification of daily Had/ERA 850 hPa geopotential height patterns for south east Africa. The nodes are referenced by two numbers (at the top of each node in figure 4.14) according to their position on the SOM. The first (second) number denotes column (row) position, for example, node [0,0] is located in the bottom left corner and node [6,4] is at the top right corner of the array. Similar synoptic circulation patterns are clustered together on the map because the mapping algorithm locates neighboring map nodes near one other in data vector space. This is an important attribute of the SOM methodology, since it allows analysis on a node by node basis and also on a map area by map area basis, as appropriate. Types representing extensive troughs and high pressure regions are apparent along with the appropriate transition of troughs and highs across the region. Nodes representing low pressure systems dominating much of the region occur on the right-hand side of the SOM array, whereas high pressure dominates the left-hand side of the SOM array. The strength of the low pressure systems decrease from right to left and top to bottom across the SOM.

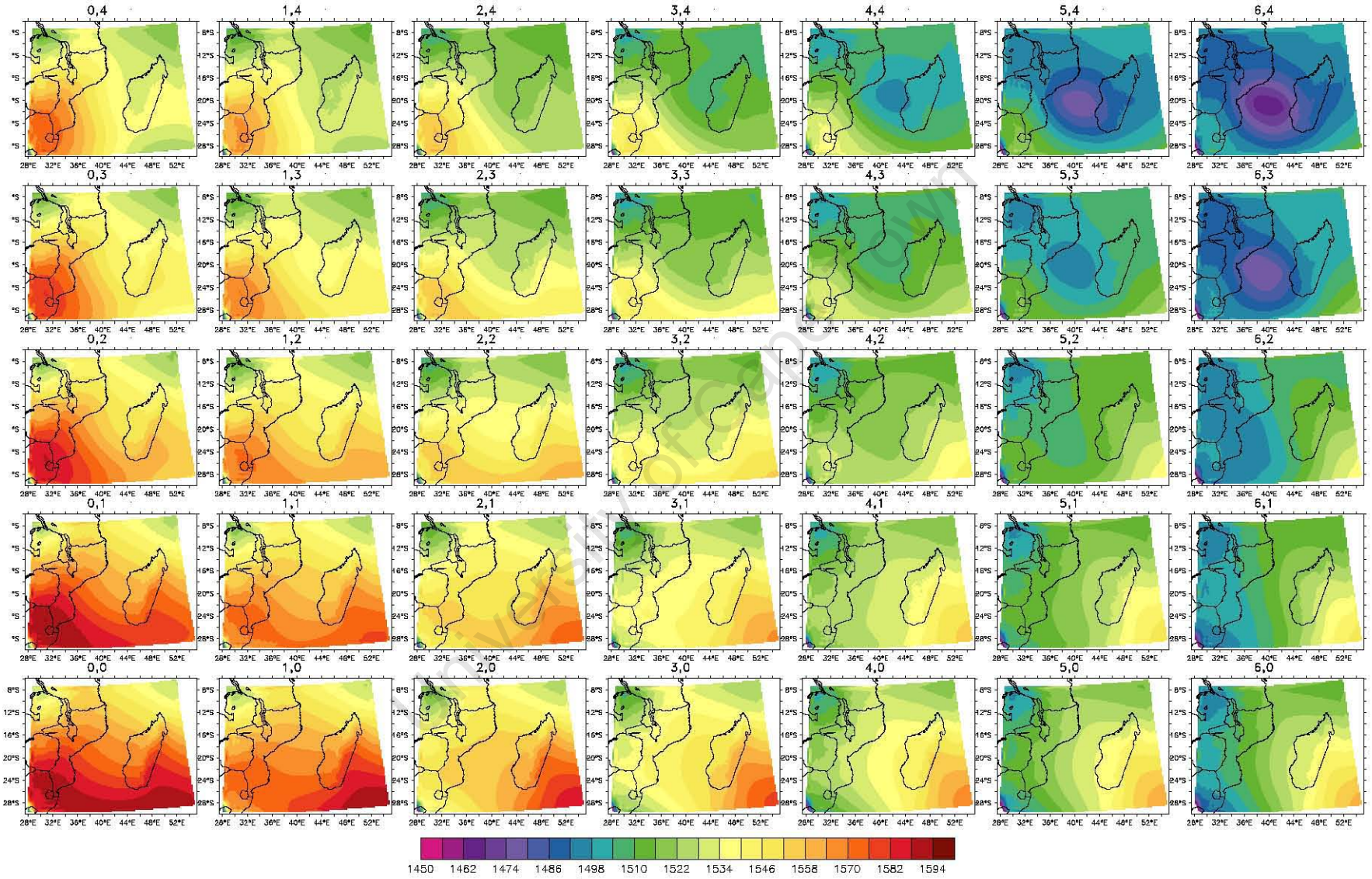

Figure 4.14: The 7x5 SOM of synoptic maps based on daily Had/ERA 850 hPa geopotential height from 1981 to 1999. The reds indicate high pressure and the cyan lower pressure. (contours are each 6 m).

After training the SOM, the data from Had/ECHAM_A2 were mapped to the SOM to determine the frequency of occurrence of each node (ie. synoptic type). The frequency of occurrence (shown as a percentage of the 6810 days analyzed) of each synoptic type during 1981 to 1999 of Had/ECHAM_A2 mapped to the trained SOM is shown in figure 4.15. Each square represents one of the nodes of the SOM (in the same orientation as in figure 4.14). The figure shows that the frequencies are distributed fairly evenly over the nodes, with relative minima in the top right and relative maxima in the bottom left of the SOM array. For example, the node [6,4] has ~67 out of 6810 (0.98%) days mapped to it while the node [0,0] had ~362 (5.32%) of the days mapped to it. The central parts of the SOM array represent transitional patterns.

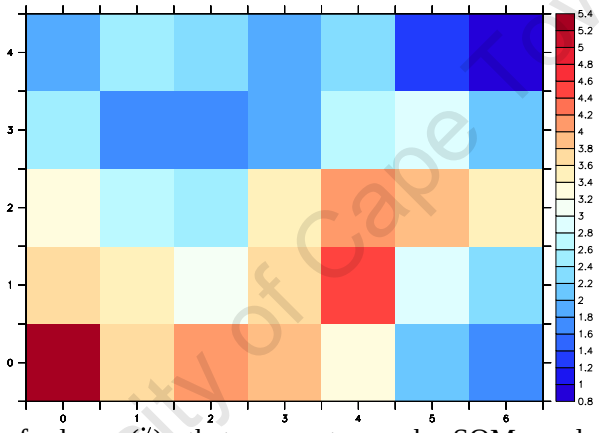

Figure 4.15: Frequency of days (%) that map to each SOM node shown in figure 4.14 (Had/ECHAM_A2). Total number of days: 6810.

Figure 4.16 shows the frequency distribution of synoptic types within each season during 1981-1999. Clear seasonality in the synoptic types is evident in figure 4.16, particularly during the summer and winter months. During summer (DJF) the highest frequencies are associated with patterns dominated by low pressure systems which tends to be mapped to the right-hand of the SOM. Patterns with deep lower pressure (nodes [6,3], [6,4], [5,4]) account for approximately 13% of the total days during DJF. This demonstrates the relatively high frequencies of cyclones over Mozambique Channel (MC) during summer seasons. Moreover, the occurrence of these synoptic types demonstrates the ability of the regional climate model HadRM3P to capture the cyclone activity over the MC. The synoptic system that frequently occurs during DJF is associated with convective cloud development. With this convective activity, rainfall and thunderstorms are typical in the northern and central por-

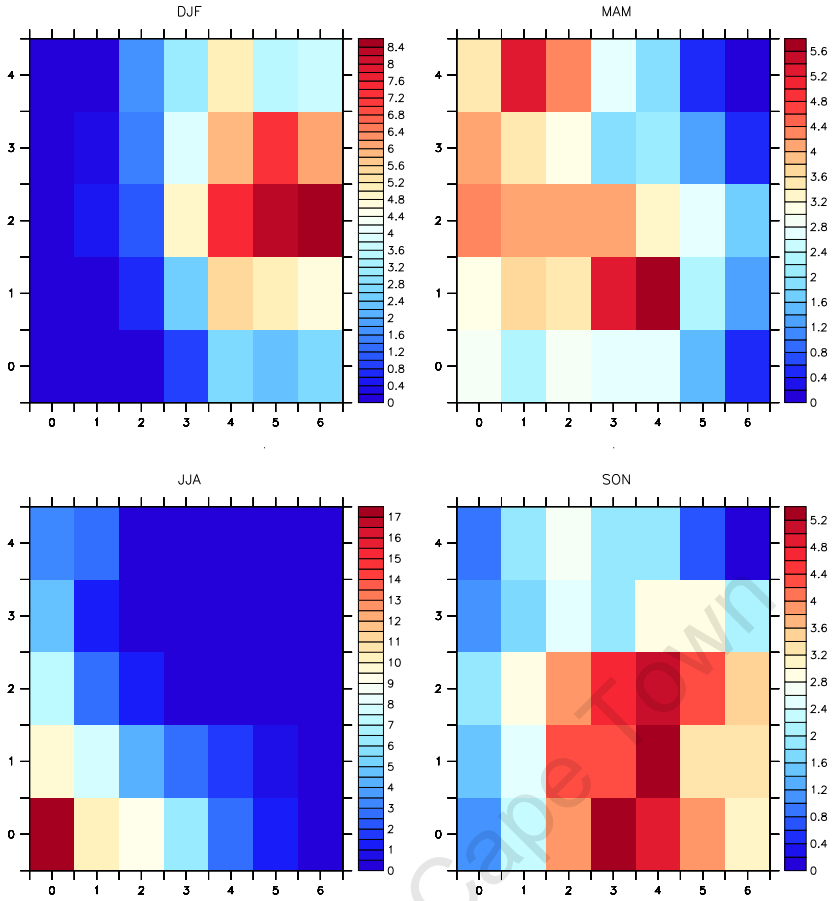

Figure 4.16: Frequency of occurrence (%) of each synoptic type during 1981-1999 on a seasonal basis (Had/ECHAM_A2). Total number of days: DJF - 1680; MAM, JJA, SON - 1710.

tions of Mozambique. On the other hand, winter types tend to map to the left-hand of the SOM. The most common winter pattern is shown by the node [0,0]. In this situation, the circulation associated with a high pressure (visible in node [0,4]) in the south dominate the weather. Due to the presence of these high pressure systems with the occurrence of continuous subsidence the region experience clear skies, calm and dry weather. In early summer (SON) and late summer (MAM) transitions periods, synoptic situations typical of either winter or summer, are evident.

To assess the biases introduced by the GCM in the synoptic types, the frequency distribution of 850 hPa geoptential hight obtained from Had/ECHAM_A2 is compared to the frequency distribution of Had/ERA (Figure 4.17). In general Had/ECHAM_A2 overstimate the most common synoptic types that frequently occur during the austral seasons. And patterns with deep low pressure system are underestimated.

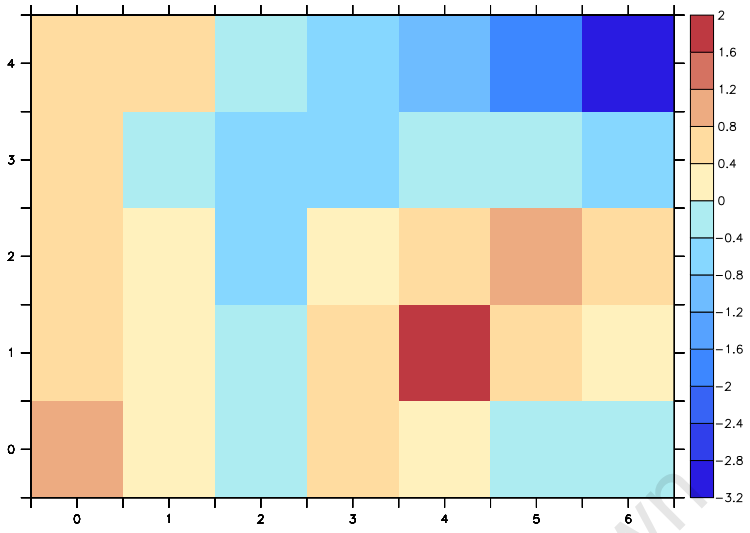

Figure 4.17: Echam bias (Had/ECHAM_A2-Had/ERA) in the frequency of occurrence of each synoptic type (shown in figure 4.14) during 1981-1999.

4.3.2 Future changes in synoptic types

Figure 4.18 presents the change in frequency (SCN-CTL) matching each synoptic type in the SOM of figure 4.14 for Had/ECHAM_A2. During DJF there are projected increase in the frequency of patterns found towards the bottom right of the SOM. These are patterns with low pressure over the country and high pressure over the ocean. Increases of these synoptic types may provide the evidence of increases in precipitation in accordance to results of the previous sections of this dissertation. However, the patterns found towards the top right of the SOM are projected to decrease. These findings may suggest a reduction of the frequency of cyclone activity by 2031-2049 during DJF. Also increases in the frequency of high pressure patterns are found, however these increases are lower compared to increases in frequency of low pressure systems. During MAM and SON higher increases in patterns found in bottom row of the SOM in figure 4.14 are found. The effect of increase of these type of patterns may explain the increases of the magnitude of upper (Tx90p, Tn90p) and lower (Tx10p, Tn10p) percentile temperature and increases in the number of dry days, especially during SON. The frequency of the patterns of higher pressure system will increase more during SON. At the same time, synoptic types of node [6,4] are expected to increase, as a result, cyclone activities may become frequent during early summer (SON). During JJA increases

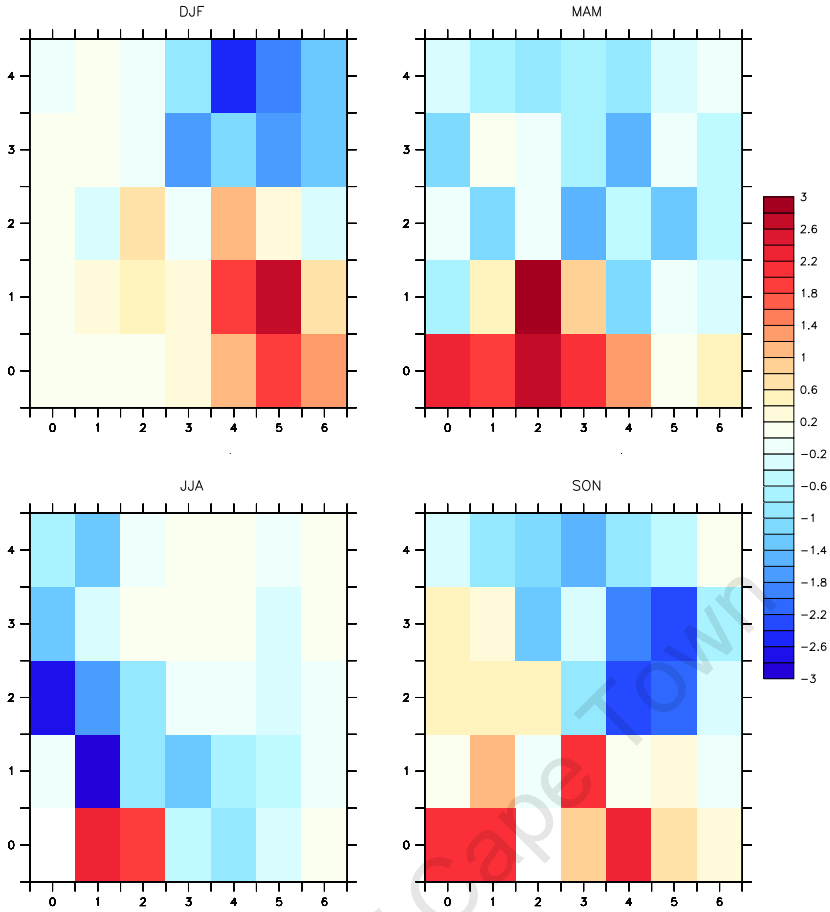

Figure 4.18: Frequency change (SCN-CTL) of each pattern (node) in figure 4.14 for Had/ECHAM_A2 simulation.

in the frequency of higher pressure systems (node [1,0], [2,0]) are found. These types of systems may be associated with increases in temperature during JJA showed previously.

CHAPTER 5

Summary and Conclusions

In many studies of climate change more attention is given to changes in means, however in the last few years changes in climate variability and extremes of weather and climate events have received increased attention (IPCC, 2007). In this study possible changes in intensity and frequency of extreme temperature and intensity of extreme precipitation in Mozambique from a regional model, was investigated using percentile and duration based indices. The regional model offers the fine horizontal resolution appropriate for capturing climate processes accurately and providing information on space scales needed for impacts analysis. The model integration has been performed using a 25 km$\times$25 km grid resolution over the area of Mozambique using two different lateral boundary condition (LBC). The following sections presents the main findings of the objectives posed in chapter 1.

Model validation

In order to estimate the model bias with respect to observational data, seasonal surface air temperature and precipitation from PRECIS system for the present climate (1981-1999) have been compared to two observational data sets (CRU and station data). It was found that the simulated patterns of temperature and precipitation in the present day are in agreement with the observations (CRU). The primary features of spatial patterns of present climate characteristics are captured by the PRECIS system. However, differences between simulation and observation are inevitable. In general there are negative biases in precipitation during summer (DJF) and late summer (MAM), and positive bias in surface air temperature (both maximum and minimum temperature) in winter (JJA) over much of the country. On the evaluation based on probability density functions (PDF), it has been shown that the PRECIS system can capture the observed PDF for each variable (T_{max},T_{min} and ppt). Across all three

variables, the model perform reasonable well in capturing the shape of the PDF. However, the problem with the model in simulating excessive light precipitation events is evident. The biases in the regional simulation at seasonal scales are present in both RCM experiments forced by ERA40 data and forced by ECHAM/OPYC3. This is observed when comparing the simulation drive by a high resolution reanalysis (ERA40) and the simulation done with the ECHAM/OPYC3. These findings suggest that the biases in the model are induced by the lateral boundary condition data or/and due to errors in the internal model physics.

Future change in extreme climate events

The second research objective posed in section 1.3 was aimed at highlight periods and locations where extremes of temperature and precipitation may potentially increase. It was found that in the future is likely to occur a positive shift in the temperature and precipitation distribution under global warming. Increases in intensity of extreme temperature (0 - 4 °C) are found all over the country with higher changes occurring in early summer (SON). The frequency of extreme temperature has different behaviour (increases/decreases) along the country and over seasons.

Noteworthy changes include more intense daily rainfall during summer in the centre of the country, associated with increases in the number of wet days (CWD) and the wetness conditions, resulting in increased probability of different extreme rainfall driven disasters (e.g. floods, erosion). These findings support the conclusions of earlier studies that a warmer climate will result in higher precipitation intensities, even in areas that in general show a tendency towards drier conditions (Meehl et al., 2007). Decreases in the number of consecutive dry days (CDD) during early summer are discernible. These changes suggest that the onset of rainfall might change to a late start, causing negative consequences to the sector of agriculture since the majority of agriculture in Mozambique is rain dependence. This knowledge could enable the adoption of strategies aimed at adapting and mitigating the effects of climate events.

Future change in synoptic types

The third objective was to link changes in the frequency and intensity of extreme events with changes in the driving atmospheric circulation. In the goal to achieve this, the self-organizing map algorithm was used to create a synoptic climatology of Mozambique during 1981-1999.

The resulting map classifies synoptic patterns, and codifies and organizes the data so that patterns that are closely located on the map show similar qualities. The results from this classification showed that circulation patterns that might be associated with high temperature (high pressure patterns) are projected to occur more frequently (increases up to 3% ~53 days of 1710 days analysed) during early and late summer. On the other hand patterns of deep low pressure - which may be associated with cyclone activities in the vicinity of Mozambique - are projected to decrease in 1 to 2.5 % (17 to 42 days of 1680 days analysed) during summer (DJF). However, low pressure patterns that may be associated with rainfall are predicted to occur more frequently during 2031-2049 compared to the period 1981-1999 for summer, based on an analysis of the HadRM3P simulations.

Limitations and further work

This study constitutes a first attempt to simulate future extreme climate change by means of a regional climate model for Mozambique and it is the first assessing climatic conditions in particular over Mozambique using high resolution (0.22°x 0.22°) RCM. However with only 19 year data available it is not possible to look at more extreme events and their relation to climate variability with any statistical confidence. It is important to note that the current analysis was based on a single model (HadRM3P) and on one scenario (SRES A2). Regional climate model predictions of regional changes in temperature and precipitation differ considerably from model to model, and regionally specific changes from a single model therefore may not be reliable. It is preferable to consider several RCMs when assessing regional climate change, and comparisons across a range of RCMs will be needed to put these results into a more robust multimodel perspective. The use of only one model implies that the results presented here should be used with caution. Also, using different forcing scenarios (e.g. SRES B2) to examine the effect of varying the scenario on the response of extreme event occurrence.

Further work could be undertaken in relation to this topic. The suggested one is to use the data produced by an ensemble of multiple dynamical and statistical downscaling models considering multiple forcing GCMs from the CMIP5 archive. This data is currently being produced by COordinated Regional climate Downscaling Experiment (CORDEX) at Climate System Analysis Group (CSAG).

Mozambique is one of the regions in Africa most vulnerable to climate change, and has the

least research in this regard. These results presented here provide a positive outlook for the development of research activities to directly meet the needs of the region.

References

Arakawa, A. and Lamb, V. R. (1977). *Computational design of the basic dynamical processes of the UCLA general circulation model*, volume 17, pages 173–265. Academic Press, New York, physics, methods in computational edition.

Ashrit, R. G., Rupa Kumar, K., and Krishna Kumar, K. (2001). ENSO-monsoon relationships in a greenhouse warming scenario. *Geophysical Research Letters*, 28:1727–1730.

Buonomo, E., Jones, R., Huntingford, C., and Hannaford, J. (2007). On the robustness of changes in extreme precipitation over Europe from two high resolution climate change simulations. *Quarterly Journal of the Royal Meteorological Society*, 133:65–81.

Christensen, J., Carter, T. R., Rummukainen, M., and Amanatides, G. (2007a). Evaluating the perfomance of regional climate models: The prudence project. *Climatic Change*, 81:1–6.

Christensen, J., Hewitson, B., Busuioc, A., Chen, A., Gao, X., Held, I., Jones, R., Kolli, R., Kwon, W.-T., Laprise, R., Magaña Rueda, V., Mearns, L., Menéndez, C., Räisänen, J., Rinke, A., Sarr, A., and Whetton, P. (2007b). *Regional Climate Projections. In: Climate Change 2007:The Physical Science Basis. Contribution of Working Group I to the Fourth Assessment Report of the Intergovernmental Panel on Climate Change*. [Solomon, S., D. Qin, M. Manning, Z. Chen, M. Marquis, K.B. Averyt, M. Tignor and H.L. Miller (eds.)].Cambridge University Press, Cambridge, United Kingdom and New York, NY, USA.

Cox, P. M., Betts, R. A., Bunton, C. B., Essery, R. L. H., Rowntree, P. R., and Smith, J. (1999). The impact of new land surface physics on the gcm simulation of climate and climate sensitivity. *Climate Dynamics*, 15:183–203.

Daikaru, K. (2006). Dynamical and thermodynimic influences on intesified daily rainfall during the asian summer monsoon under doubled atmospheric co2 conditions. *Geophysical Research Letters*, 33(L01704).

Davies, H. C. and Turner, R. H. (1977). Updating prediction models by dynamical relaxation: an examination of the technique. *Quarterly Journal of the Royal Meteorological Society*, 103:225–245.

Diffenbaugh, N. S., Pal, J. S., Trapp, R. J., and Giorgi, F. (2005). Fine-scale processes regulate the response of extreme events to global climate change. *PNAS*, 102(44):15774–15778.

DNA (1999). *Water resources of Mozambique*. Republic of Mozambique, Ministry of Public Works an Housing.

Durman, C. F., Gregory, J. M., Hassel, D. H., Jones, R. G., and Murphy, J. M. (2001). A comparison of extreme european daily precipitation simulated by a global and a regional climate model for present and future climates. *Quarterly Journal of the Royal Meteorological Society*, 127(573):1005–1015.

Dyson, L. L. and van Heerden, J. (2001). The heavy rainfall and floods over the northeastern interior of South Africa during February 2000. *South African Journal of Science*, 97:80–86.

Easterling, D. R., Meehl, G. A., Parmesan, C., Changnon, S. A., Karl, T. R., and Mearns, L. O. (2000). Climate extremes: Observations, modeling, and impacts. *Science*, 289:2068–2074.

Emori, S., Hasegawa, A., Suzuki, T., and Daikaru, K. (2005). Validation, parameterization dependence, and future projection of daily precipitation simulated with a high-resolution atmospheric GCM. *Geophysical Research Letters*, 32:L06708.

Fauchereau, N., Trzaska, S., Rouault, M., and Richard, Y. (2003). Rainfall variability and changes in southern africa during the 20th century in the global warming context. *Natural Hazards*, 29(2):139–154.

Folland, C., Karl, T., Christy, J., Clarke, R., Gruza, G., Jouzel, J., Mann, M., Oerlemans, J., Salinger, M., and Wang, S.-W. (2001). *Observed Climate Variability and Change. In: Climate Change 2001: The Scientific Basis. Contribution of Working Group I to the Third Assessment Report of the Intergovernmental Panel on Climate Change*. [Houghton, J.T., Y. Ding, D.J. Griggs, M. Noguer, P.J. van der Linden, X. Dai, K. Maskell, and C.A.

Johnson (eds.)].Cambridge University Press, Cambridge, United Kingdom and New York, NY, USA, 881pp.

Frei, C., Christensen, J., Deque, M., Jacob, D., Jones, R., and Vidale, P. (2003). Daily precipitation statistics in regional climate models: Evaluation and intercomparison for the European Alps. *Journal of Geophysical Research*, 108(D3):4124–4142.

Frei, C., Schöll, R., Fukutome, S., Schmidli, J., and Vidale, P. L. (2006). Future change of precipitation extreme in europe: Intercomparison of scenarios from regional climate models. *Journal of Geophysical Research*, 111(D06105).

Giorgi, F. (1990). Simulation of regional climate using a limited area model nested in a general circulation model. *Journal of Climate*, 3:941–964.

Giorgi, F., Bi, X., and Pal, J. S. (2004). Mean, interannual variability and trends in a regional climate change experiment over Europe, I. Present-day climate (1961–1990). *Climate Dynamics*, 22:733–756.

Giorgi, F. and Mearns, L. O. (1999). Introduction to special section: Regional climate modeling revisited. *Journal of Geophysical Research*, 104(D6):6335–6352.

Gordon, C., Cooper, C. A., Banks, H., Gregory, J. M., Johns, T. C., Mitchell, J., and Wood, R. A. (2000). The simulation of SST, sea ice extents and ocean heat transports in a version of the Hadley Centre coupled model without flux adjustments. *Climate Dynamics*, 16:147–168.

Hein-Griggs, D. M. (2008). The representation of extreme precipitation in the HadRM3P regional climate model. Master's thesis, University of Reading, Department of Meteorology.

Hewitson, B. C. and Crane, R. G. (1996). Climate downscaling: Techniques and application. *Climate Research*, 7:85–95.

Hewitson, B. C. and Crane, R. G. (2002). Self-organizing maps: applications to synoptic climatology. *Climate Research*, 22:13–26.

Hudson, D. A. and Jones, R. G. (2002). Regional climate model simulations of present-day and future climates of southern africa. Technical report, Hadley Centre Technical Note 39, Hadley Centre for Climate Prediction and Research, Met Office, Bracknell, U.K.

Huntingford, C., Jones, R. G., Prudhomme, C., Lamb, R., Gash, J. H., and Jones, D. A. (2003). Regional climate-model predictions of extreme rainfall for a changing climate. *Quarterly Journal of the Royal Meteorological Society*, 129:1607–1621.

Hurry, L. and Heerden, J. (1982). *Southern Africa's weather patterns: a guide to the interpretation of synoptic maps*. Via Afrika.

INGC (2009). Synthesis report. INGC Climate Change Report: Study on the impact of climate change on disaster risk in Mozambique. Technical report, [van Logchem B and Brito R (ed.)]. INGC, Mozambique.

IPCC (2001). *Climate Change: The Scientific Basis. Contribution of Working Group 1 to the Third Assesment Report of the Intergornmental Panel on Climate Change*. Cambridge University Press, Cambridge, United Kingdom and New York.

IPCC (2007). *Climate Change 2007: The Physical Science Basis. Contribution of Working Group I to the Fourth Assessment Report of the Intergovernmental Panel on Climate Change*. [Solomon, S., D. Qin, M. Manning, Z. Chen, M. Marquis, K.B. Averyt, M. Tignor and H.L. Miller (eds.)], Cambridge University Press, Cambridge, United Kingdom and New York, NY, USA.

Islam, S. U., Rehman, N., and Sheikh, M. M. (2009). Future change in the frequency of warm and cold spells over pakistan simulated by the precis regional climate model. *Climatic Change*, 94(1):35–45.

Jones, P., Horton, E., Folland, C., Hulme, M., Parker, D., and Basnett, T. (1999). The use of indices to identify changes in climatic extremes. *Climatic Change*, 42(1):131–149.

Jones, R., Murphy, J., and Noguer, M. (1995). Simulation of climate change over Europe using a nested regional-climate model. I: Assessment of control climate, including sensitivity to location of lateral boundaries. *Quarterly Journal of the Royal Meteorological Society*, 121:1413–1449.

Jones, R., Noguer, M., Hassell, D., Hudson, D., Wilson, S., Jenkins, G., and Mitchell, J. (2004). *Generating high resolution climate change scenarios using PRECIS*. Met Office Hadley Centre, Exeter, UK.

Katz, R. W. and Brown, B. G. (1992). Extreme events in a changing climate: Variability is more important than averages. *Climatic Change*, 21:289–302.

Katz, R. W., Brush, G., and Parlange, M. (2005). Statistics of extremes: Modeling ecological disturbances. *Ecology*, 86(5):1124–1132.

Kharin, V. V., Zwiers, F. W., and Zhang, X. (2005). Intercomparison of near surface temperature and precipitation extremes in AMIP-2 simulations, reanalyses and observations. *Journal of Climate*, 18(24):5201–5223.

Kiktev, D., Sexton, D. M. H., Alexander, L., and Folland, C. K. (2003). Comparison of modeled and observed trends in indices of daily climate extremes. *Journal of Climate*, 16:3560–3571.

Klein Tank, A. M. G. and Konnen, G. P. (2003). Trends in indices of daily temperature and precipitation extremes in Europe, 1946–99. *Journal of Climate*, 16:3665–3680.

Kohonen, T. (2001). *Self-organizing maps*. Springer.

Kohonen, T., Hynninen, J., Kangas, J., and Laaksonen, J. (1996). *SOM PAK: The Self-Organizing Map Program Package*. Laboratory of Computer and Information Science, Helsinki University of Technology, 24pp.

Leduc, M. and Laprise, R. (2009). Regional climate model sensitivity to domain size. *Climate Dynamics*, 32:833–854.

Marengo, J. A., Jones, R., Alves, L. M., and Valverde, M. C. (2009). Future change of temperature and precipitation extremes in South America as derived from the PRECIS regional climate modeling system. *International Journal of Climatology*, page n/a.

McGregor, J. L. (1997). Regional climate modelling. *Meteorology and Atmospheric Physics*, 63:105–117.

Meehl, G., Stocker, T., Collins, W., Friedlingstein, P., Gaye, A., Gregory, J., Kitoh, A., Knutti, R., Murphy, J., Noda, A., Raper, S., Watterson, I., Weaver, A., and Zhao, Z.-C. (2007). *Global Climate Projections. In: Climate Change 2007:The Physical Science Basis. Contribution of Working Group I to the Fourth Assessment Report of the Intergovernmental Panel on Climate Change*. [Solomon, S., D. Qin, M. Manning, Z. Chen,

M. Marquis, K.B. Averyt, M. Tignor and H.L. Miller (eds.)].Cambridge University Press, Cambridge, United Kingdom and New York, NY, USA.

Meehl, G. A., Karl, T., Easterling, D., Changnon, S., Pielke, R. J., et al. (2000). An introduction to trends in extreme weather and climate events: Observations, socioeconomic impacts, terrestrial ecological impacts, and model projections. *Bulletin of the American Meteorological Society*, 81:413–416.

MICOA (2007). National Adaptation Programme of Action (NAPA). Technical report, Ministry for the the Co-ordination of Environmental Affairs.

Moberg, A. and Jones, P. D. (2004). Regional climate model simulations of daily maximum and minimum near-surface temperatures across Europe compared with observed station data 1961–1990. *Climate Dynamics*, 23:695–715.

Nakicenovic, N., Alcamo, J., Davis, G., de Vries, B., Fenhann, J., Gaffin, S., Gregory, K., Grübler, A., Jung, T. Y., Kram, T., Rovere, E. L. L., Michaelis, L., Mori, S., Morita, T., Pepper, W., Pitcher, H., Price, L., Raihi, K., Roehrl, A., Rogner, H.-H., Sankovski, A., Schlesinger, M., Shukla, P., Smith, S., Swart, R., van Rooijen, S., Victor, N., and Dadi, Z. (2000). *IPCC Special Report on Emissions Scenarios*. Cambridge University Press, Cambridge, United Kingdom and New York, NY, USA.

New, M. et al. (2006). Evidence of trends in daily climate extremes over southern and west Africa. *Journal of Geophysical Research*, 111:D14102.

New, M., Hulme, M., and Jones, P. D. (1999). Representing twentieth century space time climate fields. Part I. development of a 1961-1990 mean monthly terrestrial climatology. *Journal of Climate*, 12:829–856.

New, M., Hulme, M., and Jones, P. D. (2000). Representing twentieth century space time climate fields. Part II. development of a 1961-1999 mean monthly terrestrial climatology. *Journal of Climate*, 13:2217–2238.

Nicholson, S. (1985). Sub-saharan rainfall 1981–84. *Journal of Apolied Meteorology*, 24:1388–1391.

Noguer, M., Jones, R., and Murphy, J. M. (1998). Sources of systematic errors in the climatology of a regional climate model over Europe. *Climate Dynamics*, 14(10):691–712.

Oberhuber, J. (1993). Simulation of the atlantic circulation with a coupled sea-ice mixed layer-isopycnal general circulation model. Part I: model description. *Journal of Physical Oceanography*, 13:808–829.

Perkins, S. E., Pitmanm, A. J., Holbrook, N. J., and McAneney, J. (2007). Evaluation of the AR4 climate models simulated daily maximum temperature, minimum temperature, and precipitation over australia using probability density functions. *Journal of Climate*, 20:4356–4373.

Pesquero, J. F., Chou, S. C., Nobre, C. A., and Marengo, J. A. (2009). Climate downscaling over South America for 1961–1970 using the Eta Model. *Theoretical and Applied Climatology*, 99(1-2):75–93.

Plummer, N., Salinger, M. J., Nicholls, N., Suppiah, R., Hennessy, K. J., Leighton, R. M., Trewin, B., Page, C. M., and Lough, J. M. (1999). Changes in climate extremes over the australian region and new zealand during the twentieth century. *Climatic Change*, 42(1):183–202.

Roeckner, E., Arpe, K., Bengtsson, L., Christoph, M., Claussen, M., Dümenil, L., Esch, M., Giorgetta, M., Schlese, U., and Schulzweida, U. (1996). The atmospheric general circulation model ECHAM-4: model description and simulation of present-day climate. Technical Report 218, Max- Planck Institute for Meteorology, Hamburg, Germany, 90 pp.

Rupa Kumar, K., Sahai, A. K., Krishna Kumar, K., Patwardhan, S., Mishra, P. K., Revadekar, J. V., and Kamala, K. (2006). High-resolution climate change scenarios for india for the 21stcentury. *Current Science*, 90(3):334–345.

Solman, S. A., Nuñez, M. N., and Cabré, M. F. (2008). Regional climate change experiments over southern South America. I: present climate. *Climate Dynamics*, 30(5):533–552.

Stainforth, D. A., Allen, M. R., Tredger, E. R., and Smith, L. A. (2007). Confidence, uncertainty and decision-support relevance in climate predictions. *Philosophical Transactions of The Royal Society A*, 365:2145–2161.

Tadross, M. A. (2009). Climate change modelling and analyses for Mozambique. Technical report, Final report detailing the support provided to the Instituto Nacional de Gestão de Calamidades (INGC) adaptation to climate change project.

Tadross, M. A., Jack, C., and Hewitson, B. C. (2005). On RCM-based projections of change in southern African summer climate. *Geophys. Res. Lett.*, 32:L23713.

Tebaldi, C., Hayhoe, K., Arblaster, J., and Meehl, G. (2006). Going to the extremes; an inter-comparison of model-simulated historical and future changes in extreme events. *Climatic Change*, 79:185–211.

Tyson, P. and Preston-White, R. A. (2000). *The weather and climate of southern Africa*. Oxford University Press, Cape Town.

Uppala, S., Kållberg, P., Simmons, A., Andrae, U., Bechtold, V., Fiorino, M., Gibson, J., Haseler, J., Hernandez, A., Kelly, G., Li, X., Onogi, K., Saarinen, S., Sokka, N., Allan, R., Andersson, E., Arpe, K., Balmaseda, M., Beljaars, A., Berg, L., Bidlot, J., Bormann, N., Caires, S., Chevallier, F., Dethof, A., Dragosavac, M., Fisher, M., Fuentes, M., Hagemann, S., Hólm, E., Hoskins, B., Isaksen, L., Janssen, P., Jenne, R., McNally, A., Mahfouf, J.-F., Morcrette, J.-J., Rayner, N., Saunders, R., Simon, P., Sterl, A., Trenberth, K., Untch, A., Vasiljevic, D., Viterbo, P., and Woollen, J. (2005). The era-40 re-analysis. *Quarterly Journal of the Royal Meteorological Society*, 131:2961–3012.

Vincent, L. A., Peterson, T. C., Barros, V. R., Marino, M. B., Rusticucci, M., Carrasco, G., Ramirez, E., et al. (2005). Observed trends in indices of daily temperature extremes in South America 1960-2000. *Journal of Climate*, 18(23):5011–5023.

Wehner, M. F. (2004). Predicted twenty-first-century changes in seasonal extreme precipitation events in the parallel climate model. *Journal of Climate*, 17:4281 – 4290.

Wilby, R. L., Charles, S. P., Zorita, E., Timbal, B., Whetton, P., and Mearns, L. O. (2004). *Guidelines for Use of Climate Scenarios Developed from Statistical Downscaling Methods.*, page 27pp. IPCC Data Distribution Centre, University of East Anglia, U.K.

Wilby, R. L. and Wigley, T. (1997). Downscaling general circulation model output: a review of methods and limitations. *Progress in Physical Geography*, 21:530–548.

Wilson, S., Hassell, D., Hein, D., Jones, R., and Taylor, R. (2008). *Installing and using the Hadley Centre regional climate modelling system, PRECIS Version 1.7*.

Xu, Y., Huang, X., Zhang, Y., Lin, W., and Lin, E. (2006). Statistical analyses of climate change scenarios over China in the 21st century. *Advances in Climate Change Research*, (Suppl. 1):50–53.

Yarnal, B. (1993). *Synoptic Climatology in Environmental Analysis: A Primer*. Belhaven Press: London.

Zhang, Y., Yinlong, X., Wenjie, D., Lijuan, C., and Sparrow, M. (2006). A future climate scenario of regional changes in extreme climate events over China using the PRECIS climate model. *Geophysical Research Letters*, 33:L24702.

A P P E N D I X

APPENDIX A

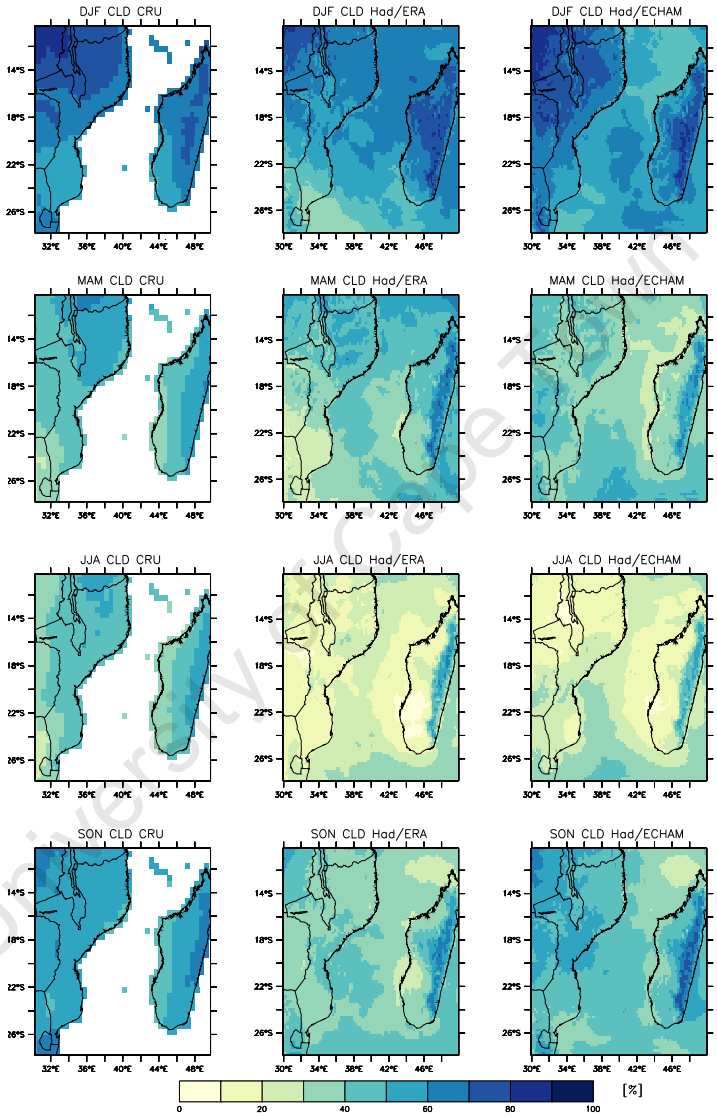

Figure A.1: Total cloud cover (%) for CRU (*left*), Had/ERA (*center*) and Had/ECHAM_A2 (*right*) for each of the four seasons.

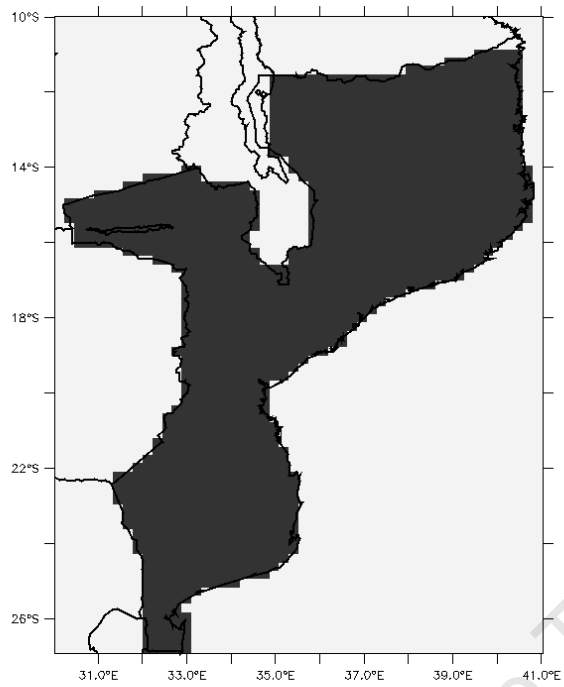

Figure A.2: Mask used before compute the PDFs from the RCM outputs. Only values inside the grey area were used.

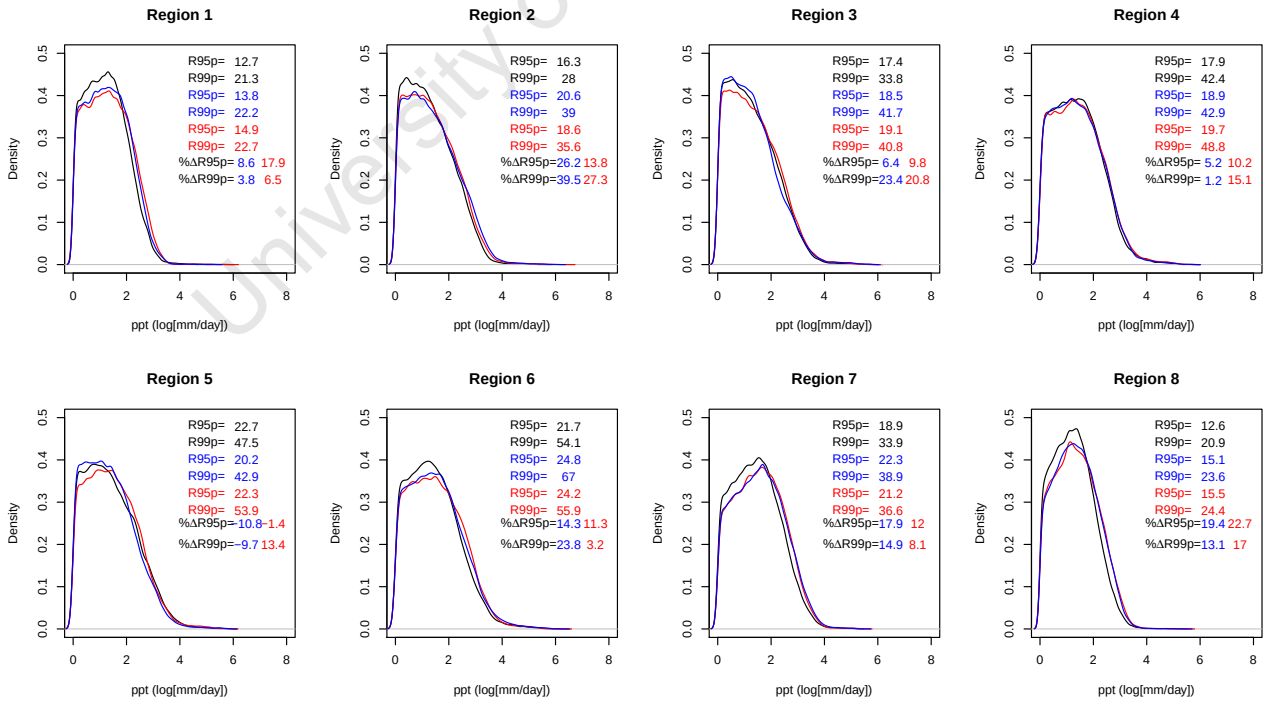

Figure A.3: Daily total precipitation probability distribution function for MAM in CTL (1981-1999, black), MDL (2011-2029, blue) and SCN (2031-2049, red) simulations

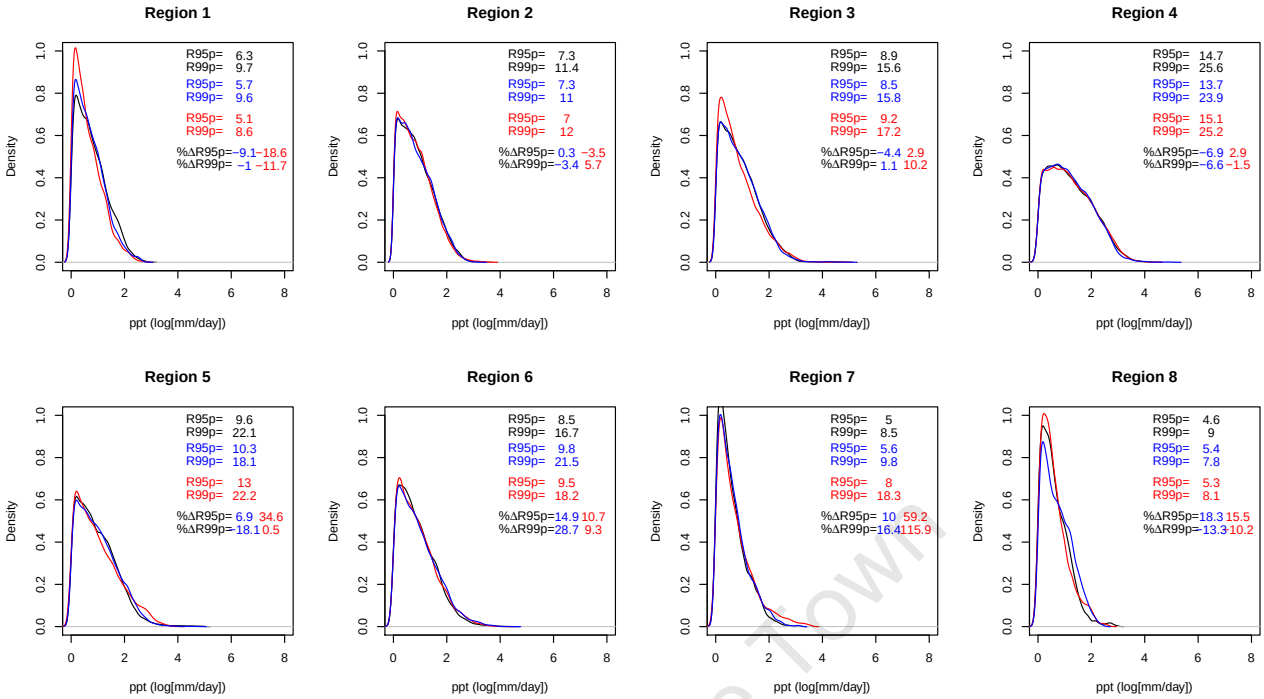

Figure A.4: Daily total precipitation probability distribution function for JJA in CTL (1981-1999, black), MDL (2011-2029, blue) and SCN (2031-2049, red) simulations

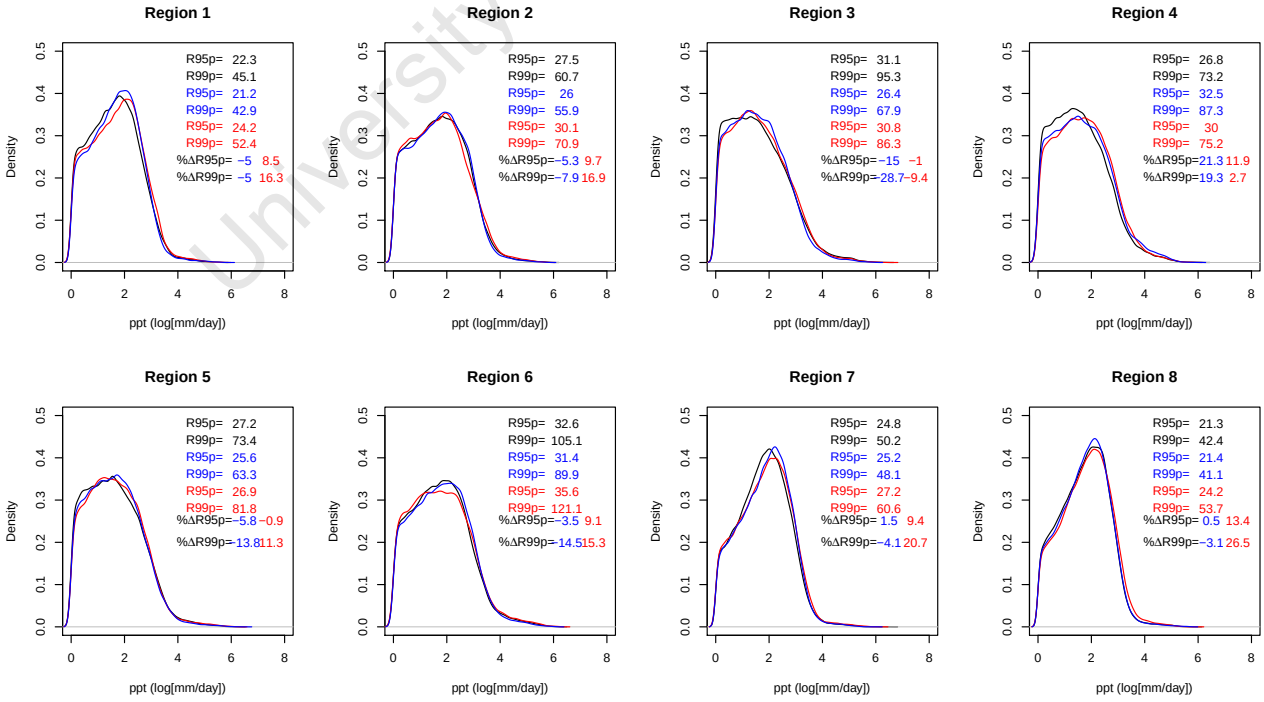

Figure A.5: Daily total precipitation probability distribution function for SON in CTL (1981-1999, black), MDL (2011-2029, blue) and SCN (2031-2049, red) simulations